Euro. Jnl of Applied Mathematics: page 1 of 28 © Cambridge University Press 2017
doi:10.1017/S0956792517000067

Sharp-interface formation during lithium intercalation into silicon

E. MECA[1], A. MÜNCH[2] and B. WAGNER[1,3]

[1]*Weierstrass Institute, Mohrenstraße 39, 10117 Berlin, Germany*
email: meca@wias-berlin.de
[2]*Mathematical Institute, University of Oxford, Andrew Wiles Building, Woodstock Road, Oxford, OX2 6GG UK*
email: muench@maths.ox.ac.uk
[3]*Technische Universität Berlin, Institute of Mathematics, Straße des 17. Juni 136, 10623 Berlin, Germany*
email: wagnerb@wias-berlin.de

(*Received 17 May 2016; revised 24 February 2017; accepted 1 March 2017*)

In this study, we present a phase-field model that describes the process of intercalation of Li ions into a layer of an amorphous solid such as amorphous silicon (a-Si). The governing equations couple a viscous Cahn–Hilliard-Reaction model with elasticity in the framework of the Cahn–Larché system. We discuss the parameter settings and flux conditions at the free boundary that lead to the formation of phase boundaries having a sharp gradient in lithium ion concentration between the initial state of the solid layer and the intercalated region. We carry out a matched asymptotic analysis to derive the corresponding sharp-interface model that also takes into account the dynamics of triple points where the sharp interface intersects the free boundary of the Si layer. We numerically compare the interface motion predicted by the sharp-interface model with the long-time dynamics of the phase-field model.

Key words: Asymptotic Analysis, Phase-Field Model, Stability Analysis, Interface Dynamics, Numerical Methods

1 Introduction

Silicon electrodes for lithium-ion batteries are currently the subject of very intense research to make silicon a practical alternative to graphite. Silicon can store a large amount of lithium, but the large stresses that these electrodes undergo tend to cause their fracture and pulverization after a few cycles. Various investigations to circumvent these problems have led to designs of nanostructured electrodes such as arrays of pillars or nanowires.

However, in order to carry out systematic and knowledge-based optimizations a fundamental understanding of the mechanisms involved in the intercalation process of silicon itself is needed. This has led to a number of experimental and theoretical investigations, partly with, seemingly, contradictory results. In particular, the experiments of Sethuraman *et al.* [29] on the stress evolution of a silicon electrode during intercalation have had a great impact on the modelling of silicon electrodes, as they have been taken as a proof of the surprising result that lithiated amorphous silicon behaves plastically, see, for example, the analysis in [3]. Their analysis is based on the assumption that the film of amorphous

Downloaded from https://www.cambridge.org/core. Universitaetsbibliothek, on 26 Oct 2017 at 13:20:02, subject to the Cambridge Core terms of use, available at https://www.cambridge.org/core/terms. https://doi.org/10.1017/S0956792517000067

silicon is thin enough with respect to the substrate to which it is attached, so that the stress can be assumed uniform in the whole amorphous silicon film. However, while the thickness of the film can be controlled, the uniformity of the stress is an unknown. In fact, it has been shown recently in [15] and [25] that the assumption of uniformity of the stress can indeed obscure the interpretation of the results.

In addition, as has been shown more recently in [19], the theoretical yield stress is never reached, which has led to some phenomenological modelling to explain yielding [34], sometimes also discarding plasticity [19]. On the other hand, the models used to take into account plasticity have problems in the determination of the parameters, sometimes suggesting a power law with exponent as high as 50 for the constitutive law [5], which can be taken as a hint that the model may not be complete. Further analysis for different electrode geometries involving cylindrical and spherical silicon particles as well as annular structures have been carried out to investigate stress evolution and deformation of lithiated silicon, see [7, 8, 10].

On the other hand, regarding the structural properties of silicon, it is known that after the first intercalation cycle, the original crystalline silicon becomes amorphous, see the review by McDowell *et al.* [22] and references therein. Moreover, as it has been shown in [21] and [31], the first intercalation of crystalline as well as amorphous silicon occurs through a two-phase mechanism. For subsequent intercalation cycles, in the case of amorphous silicon, the question of whether this two-phase process is also present has been raised in [20, 21]. A recent study by Cubuk & Kaxiras [9] based on molecular dynamics simulations relates the two-phase lithiation of amorphous silicon with a sharp structural transition in amorphous Li_xSi for $x \approx 2$ between a phase in which the Li atoms are embedded in a covalent silicon matrix to a phase in which Si atoms are packed in small clusters with few covalent bonds between them, surrounded by a dense, amorphous structure of Li atoms, suggesting a transition from a mechanically Si-like phase to a softer Li-like phase.

In [23], a phase-field model that couples a viscous Cahn–Hilliard-Reaction model with elasticity has been derived to describe the process of intercalation of Li-ions into a layer of amorphous silicon and investigate conditions leading in the long-time limit to the formation of sharp phase boundaries between the original silicon phase and the lithiated phase. The analysis of the long-time dynamics of the emerging sharp phase boundaries is the subject of the present study.

In order to study the long-time dynamics of the system, we derive a sharp-interface model by using matched asymptotics. While this technique has not been used for this particular application, the analysis of similar models has been undertaken in the past [1, 12–14,16]. Nevertheless, no study has considered complex non-linear boundary conditions, such as the ones that are relevant for the problem at hand, which we consider in detail.

After presenting the phase-field formulation in Section 2, we show in the remainder of this paper how an intercalation process is nucleated, for example, due to some defect on the free absorbing boundary of a layer (or nanowire), and upon reaching a critical lithium concentration, a phase transition sets in, which, in turn, leads to a sharp phase boundary that then moves into the bulk of the layer and along its free boundary.

In Section 3, we derive for this regime a sharp-interface model using matched asymptotic expansions, whereby the analysis is divided into three regions, the sharp interface analysis

Downloaded from https://www.cambridge.org/core. Universitaetsbibliothek, on 26 Oct 2017 at 13:20:02, subject to the Cambridge Core terms of use, available at https://www.cambridge.org/core/terms. https://doi.org/10.1017/S0956792517000067

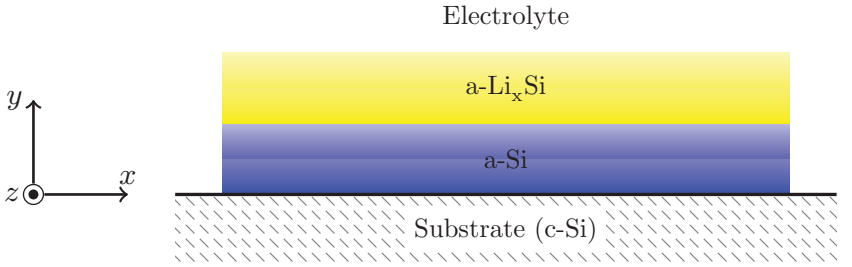

FIGURE 1. Schematic of the system.

in the bulk of the layer, the analysis close to the free boundary and the analysis of the triple points, where the sharp interface intersects the free boundary of the silicon layer. All three regions have to be matched and finally yield the sharp-interface model. Finally, we investigate numerically in Section 4 the dynamics of the long-time limit of the phase-field model and compare the evolution of the emerging phase boundaries with the expression for the velocities found from matched asymptotic analysis.

2 Formulation of the phase-field model

The system we consider consists of a thin layer of amorphous silicon resting on an undeformable substrate (see Figure 1). Lithium enters the layer as a consequence of the difference of electrochemical potential with the electrolyte. As the lithium concentration is increased, the layer experiences a phase transformation from a poorly lithiated phase (a-Si) to a heavily lithiated one (Li_xSi with x> 2). Lithium insertion causes a stress-free strain. For a discussion of the effect of this phase transformation on stress in this process, we have formulated a mathematical model in [23] and we will briefly introduce the complete phase-field model here.

To facilitate the discussion of the results, we confine our description of elasticity to linear elasticity and follow the standard approach to the coupling of phase transitions with linear elasticity, see, e.g., [11] for details. From Hooke's law, the elastic energy is given by

$$W = \frac{1}{2} C_{ijkl} \left(\epsilon_{ij} - \epsilon^0_{ij}\right) \left(\epsilon_{kl} - \epsilon^0_{kl}\right), \tag{2.1}$$

where $1 \leqslant i, j, k, l \leqslant 3$ and the fourth-order tensor C_{ijkl} is defined as the *elasticity tensor* or as the *stiffness tensor*, ϵ_{ij} denotes the *strain tensor*

$$\epsilon_{ij} = \frac{1}{2} \left(\partial_j u_i + \partial_i u_j\right), \tag{2.2}$$

defined by the *displacement field* **u**, as the difference between the actual position of a material point and the position in the undeformed material **x** (reference configuration). The *stress-free strain tensor*, that is, the strain due, e.g., to composition changes in the absence of stress, is assumed to grow linearly with the concentration of lithium atoms c:

$$\epsilon^0_{ij} = \alpha \left(c - \bar{c}\right) \delta_{ij}, \tag{2.3}$$

Downloaded from https://www.cambridge.org/core. Universitaetsbibliothek, on 26 Oct 2017 at 13:20:02, subject to the Cambridge Core terms of use, available at https://www.cambridge.org/core/terms. https://doi.org/10.1017/S0956792517000067

where α and $\bar{c}$ are constants, possibly depending on the phase. Note that this choice implies an isotropic strain change with concentration, but this needs not to be the case and more general relations are possible. In the following, the *plane-strain* approximation is used, meaning that $u_3 = 0$ and there is no dependence on z, hence $\epsilon_{ij} = 0$ for $i = 3$ or $j = 3$. Nevertheless, note that in general $\epsilon^0_{33} \neq 0$ and hence we retain the range of the indices.

Using the symmetries of C_{ijkl}, the choice of elastic energy implies for the *stress tensor*

$$\sigma_{ij} = C_{ijkl}\left(\epsilon_{kl} - \epsilon^0_{kl}\right), \tag{2.4}$$

and assuming that the timescale of the elastic relaxation is much faster than that of diffusion or the phase transformation, elastic equilibrium implies that the divergence of the stress tensor is zero:

$$\partial_j \sigma_{ij} = 0. \tag{2.5}$$

Equation (2.5) will have to be fulfilled separately at each phase in the layer and it can be written explicitly in terms of the displacement field using

$$\sigma_{ij} = \frac{E}{1+\nu}\left(\epsilon^M_{ij} + \frac{\nu}{1-2\nu}\epsilon^M_{kk}\delta_{ij}\right), \tag{2.6}$$

where E is *Young's modulus*, ν is *Poisson's ratio* and $\epsilon^M_{ij} = \epsilon_{ij} - \epsilon^0_{ij}$ is the *mechanical strain*, the difference between the strain tensor and the stress-free strain tensor.

For the present problem, the elastic properties of both phases are assumed different. We limit this difference to Young's modulus, since according to [30], there is no clear tendency in the variation of ν, which therefore will not depend on c. This, together with equations (2.2), (2.3) and (2.6) lead to the following form of equation (2.5) in terms of the displacement field, after multiplying it by a factor $(1+\nu)/E$:

$$\begin{aligned}\frac{1}{2}\frac{E'}{E}\nabla c\left(\nabla\mathbf{u} + \nabla\mathbf{u}^T\right) - \frac{E'}{E}\frac{1+\nu}{1-2\nu}\alpha(c-\bar{c})\nabla c + \frac{E'}{E}\frac{\nu}{1-2\nu}\left(\nabla\cdot\mathbf{u}\right)\nabla c \\ + \frac{1}{2}\nabla^2\mathbf{u} + \frac{1}{2(1-2\nu)}\nabla\left(\nabla\cdot\mathbf{u}\right) - \alpha\frac{1+\nu}{1-2\nu}\nabla c = 0,\end{aligned} \tag{2.7}$$

where E' is the derivative of Young's modulus with respect to concentration c.

For the transport of concentration c, we use the viscous Cahn–Hilliard model

$$\partial_t c = \nabla\cdot\left(M(c)\nabla\left(\mu + \chi\,\varepsilon\,\partial_t c\right)\right), \tag{2.8}$$

where $M(c)$ is the *mobility function*, which in the present study is taken to be a constant. The last term is the *viscous term*, see [26] and $\chi \geqslant 0$ corresponds to a parameter with dimensions of viscosity. The chemical potential

$$\mu = \frac{1}{N_\Omega}\frac{\delta\mathcal{F}}{\delta c} = -\gamma\varepsilon\,\nabla^2 c + \frac{\gamma}{\varepsilon}\frac{1}{2}c(1-c)(1-2c) + \partial_c W(\epsilon_{ij}, c), \tag{2.9}$$

is the variational derivative of the free energy

$$\mathcal{F} = N_\Omega\int_\Omega \frac{1}{2}\gamma\varepsilon\,|\nabla c|^2 + \frac{\gamma}{\varepsilon}f(c) + W(\epsilon_{ij}, c)\,, \tag{2.10}$$

Downloaded from https://www.cambridge.org/core. Universitaetsbibliothek, on 26 Oct 2017 at 13:20:02, subject to the Cambridge Core terms of use, available at https://www.cambridge.org/core/terms. https://doi.org/10.1017/S0956792517000067

where $f(c)$ is the usual double-well potential (free energy per particle) and $W(\epsilon_{ij}, c)$ is the elastic energy as defined in equation (2.1) for an isotropic elasticity tensor. The constant γ carries the dimensions of energy times length, and N_Ω is the number of diffusion sites per unit volume. The parameter ε is related with the interface width and the interfacial energy between the lithiated and the unlithiated phases.

We non-dimensionalize equations (2.7) and (2.8) via

$$\mu = \mu^* \gamma H_0^{-1},\ x = x^* H_0,\ y = y^* H_0,\ t = t^* H_0^3 M^{-1} \gamma^{-1},\ \varepsilon = \varepsilon^* H_0,$$

denoting with * the non-dimensionalized variables. The characteristic length scale H_0 corresponds to the height of the layer and M is the constant mobility. For the elastic variables, we apply the scalings

$$C_{ijkl} = C^*_{ijkl} \frac{E_{\mathrm{Si}}}{2(1+\nu)},\ u_i = u_i^* \alpha H_0,\ \epsilon_{ij} = \epsilon_{ij}^* \alpha,\ \sigma_{ij} = \sigma_{ij}^* \frac{\alpha E_{\mathrm{Si}}}{2(1+\nu)}.$$

After dropping the *, the non-dimensionalized problem can be written as

$$\partial_t c = \nabla^2 \left(\mu + \varepsilon\beta\, \partial_t c\right), \tag{2.11a}$$

$$\mu = -\varepsilon \nabla^2 c + \frac{1}{\varepsilon} f'(c) + \delta\, \partial_c W\left(\epsilon_{ij}, c\right), \tag{2.11b}$$

$$\partial_j \sigma_{ij} = 0, \tag{2.11c}$$

$$\sigma_{ij} = 2G\left(\epsilon_{ij} - \epsilon^0_{ij}\right) + \frac{2\nu}{1-2\nu} G\left(\epsilon_{kk} - \epsilon^0_{kk}\right)\delta_{ij}, \tag{2.11d}$$

where the constitutive laws for the non-dimensional shear modulus $G(c) = E(c)/E_{\mathrm{Si}}$ and stress-free strain $\epsilon^0_{ij}(c)$ are specified as

$$G(c) = 1 + g(c)\left(\frac{E_{\mathrm{Li_xSi}}}{E_{\mathrm{Si}}} - 1\right), \quad \epsilon^0_{ij}(c) = h(c)\delta_{ij}, \tag{2.11e}$$

and the derivative of the non-dimensional elastic energy takes the form

$$\begin{aligned}\partial_c W(\epsilon_{ij}, c) = {} & \frac{(1-\nu)G'(c)}{1-2\nu}\left(\partial_1 u_1^2 + \partial_2 u_2^2\right) + \frac{1}{2}G'(c)\left(\partial_1 u_2 + \partial_2 u_1\right)^2 \\ & + \frac{2\nu G'(c)}{1-2\nu}\partial_1 u_1 \partial_2 u_2 - \frac{2(1+\nu)}{1-2\nu}(h(c)G(c))'\nabla\cdot\mathbf{u} \\ & + \frac{3(1+\nu)}{1-2\nu}\left(h(c)^2 G(c)\right)'.\end{aligned} \tag{2.11f}$$

Here, $h(c)$ and $g(c)$ are interpolating functions such that $g(0) = h(0) = 0$ and $g(1) = h(1) = 1$. Note that we have slightly generalized our previous choice (2.3) for ϵ^0_{ij}, while letting $\bar{c} = 0$. Also, note that we have not defined a scaling for c, but this should define 0 and 1 to be the two equilibrium concentrations. For the boundaries in contact with the substrate, we will take a no-flux/no-deformation boundary condition:

$$\mathbf{u} = 0,\ \mathbf{n}\cdot\nabla c = 0,\ \mathbf{n}\cdot\nabla\mu = 0, \tag{2.11g}$$

where $\mathbf{n}$ is the normal vector to the surface. In the case of the boundaries in contact with

Downloaded from https://www.cambridge.org/core. Universitaetsbibliothek, on 26 Oct 2017 at 13:20:02, subject to the Cambridge Core terms of use, available at https://www.cambridge.org/core/terms. https://doi.org/10.1017/S0956792517000067

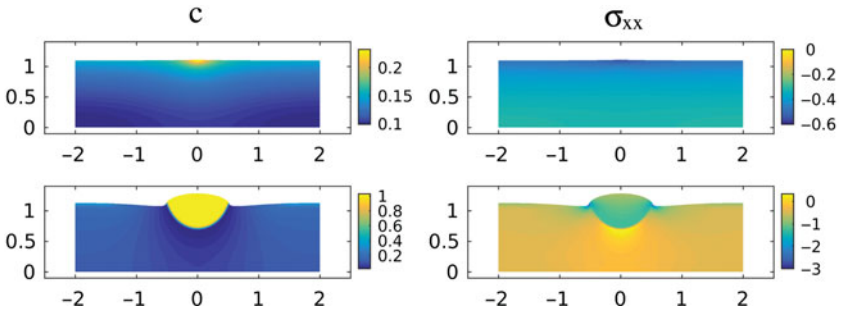

FIGURE 2. Effect of a localized non-uniformity of the flux. Top: Concentration and σ_{xx} at $t = 0.027$. Bottom: Concentration and σ_{xx} at $t = 0.037$. We use the constant flux boundary condition and the parameters are as follows: $\beta = 0.5$ and $\delta = 0.1$. (non-dimensional units, the deformation has been scaled to obtain a better visualization).

the electrolyte, we take a no-traction boundary condition and, following [6], assume a consistent no-flux condition for c (also known as *variational boundary condition*), together with a non-linear absorption condition for the chemical potential [33][1]

$$\sigma \cdot \mathbf{n} = 0, \ \mathbf{n} \cdot \nabla c = 0, \ \mathbf{n} \cdot \nabla \mu = K(\mu) = k\left(1 - e^{Q(\mu - \mu_{\text{ext}})}\right), \tag{2.11h}$$

where, μ_{ext} is scaled like μ. Other than this absorption condition, we will also consider the constant flux boundary conditions $\mathbf{n} \cdot \nabla \mu = k$.

The problem thus depends on the following non-dimensional constants:

$$\beta = \frac{\chi M}{H_0}, \quad k = \frac{k_r H_0^2}{M\gamma}, \quad \delta = \frac{H_0 E_{\text{Si}} \alpha^2}{2(1+\nu)\gamma}, \quad Q = \frac{\gamma H_0^{-1}}{k_B T}. \tag{2.12}$$

with the elastic ratio $E_{\text{Li}_x\text{Si}}/E_{\text{Si}}$ and ν, together with the parameter μ_{ext} and ε. Note that Q and k play a similar role in the vicinity of equilibrium, and δ is the ratio of elastic to interfacial energies.

For the numerical simulations, we have used $E_{\text{Li}_x\text{Si}}/E_{\text{Si}} = 4/9$ and $\nu = 0.25$, in accordance with the calculations form [30]. We also use $\varepsilon = 0.005$ and $k = 4.0$ except where indicated.

3 Sharp-interface asymptotics

In a typical scenario, small defects on the free interface lead to preferred absorption sites of the incoming ions. The critical concentration that initiates the phase transition is reached in these sites first and leads to the local formation of sharp phase boundaries and the growth of lithiated regions. In Figure 2 are displayed snapshots of such an event (see Section 4 below and Ref. [23] for more information on the numerics). It shows the concentration and σ_{xx} before and after the formation of the sharp interface in the presence of a non-uniform flux. In this case, we have taken the flux in a small region near $x = 0$ to be approximately two times the value outside of it.

[1] It is currently being discussed whether this Butler–Volmer-type boundary condition is appropriate, as opposed to generalized Marcus kinetics. See [2] for details.

Downloaded from https://www.cambridge.org/core. Universitaetsbibliothek, on 26 Oct 2017 at 13:20:02, subject to the Cambridge Core terms of use, available at https://www.cambridge.org/core/terms. https://doi.org/10.1017/S0956792517000067

On top of Figure 2, there is a characteristic concentration pattern just before phase separation. Near $x = 0$ the concentration is higher than elsewhere, but this is not so clearly reflected in the stress field, dominated by a vertical gradient. The stress is more compressive near the top, where the concentration is the highest. Once phase separation takes place a sharp interface is created. In Figure 2 (bottom), the corresponding cross-sections are shown. Now the deformation is much more visible, as we have two distinct phases with concentrations near $c = 1$ and $c = 0$. We see how σ_{xx} is more negative in the transformed phase, indicating a strong compression and this compression is highest near the triple junctions. In this example, we have prescribed a constant flux as in [23], and taken lateral periodic boundary conditions for simplicity.

It will be difficult to analyse systematically these nucleation and growth processes, where diffusion, elasticity and interfacial effects are present and hard to disentangle using the present model. However, in the past it has been shown to be insightful to derive reduced sharp-interface models describing the dynamics asymptotically.

To our knowledge, the first development of this kind for a similar problem (an Allen–Cahn equation coupled with non-linear elasticity) was made by Fried & Gurtin [12]. They did a comprehensive study and developed a Gibbs–Thomson equation that incorporates the right *Eshelby Traction*.

The original reference for the analysis of our problem (i.e. the Larché–Cahn system, understood as a Cahn–Hilliard equation coupled with linear elasticity) is [16]. The authors compare the results with a boundary integral approach and write explicitly the correspondence between the sharp and the diffuse interface models. According to their result, the elastic term in the chemical potential has to have a particular scaling with the interface width in order to recover instantaneous diffusion away from the interface. Also, they find out that for that purpose, the interpolating functions of c that define E and ϵ^0_{ij} must fulfil some conditions.

Further analysis has been performed since then. For instance, Garcke [13] proved some existence and uniqueness results for the diffuse interface model, followed by an asymptotic analysis [14], finding the corresponding sharp-interface model. More recently, Abels & Schaubeck [1] have proven rigorously these asymptotic results. However, none of these studies considers realistic boundary conditions.

3.1 Sharp interface in the bulk

We begin our study of the sharp-interface asymptotics with the study of the sharp interface in the bulk, i.e. the boundary between lithiated and non-lithiated silicon, see Figure 3.

3.1.1 *Outer expansion*

$$c(x, y, t) = c_0 + \varepsilon c_1 + \varepsilon^2 c_2 + \cdots, \tag{3.1a}$$

$$\mu(x, y, t) = \varepsilon^{-1}\mu_{-1} + \mu_0 + \varepsilon\mu_1 + \cdots, \tag{3.1b}$$

$$u_i(x, y, t) = u_{i,0} + \varepsilon u_{i,1} + \varepsilon^2 u_{i,2} + \cdots, \tag{3.1c}$$

$$\sigma_{ij}(x, y, t) = \varepsilon^{-1}\sigma_{ij,-1} + \sigma_{ij,0} + \varepsilon\sigma_{ij,1} + \varepsilon^2\sigma_{ij,2} + \cdots. \tag{3.1d}$$

Downloaded from https://www.cambridge.org/core. Universitaetsbibliothek, on 26 Oct 2017 at 13:20:02, subject to the Cambridge Core terms of use, available at https://www.cambridge.org/core/terms. https://doi.org/10.1017/S0956792517000067

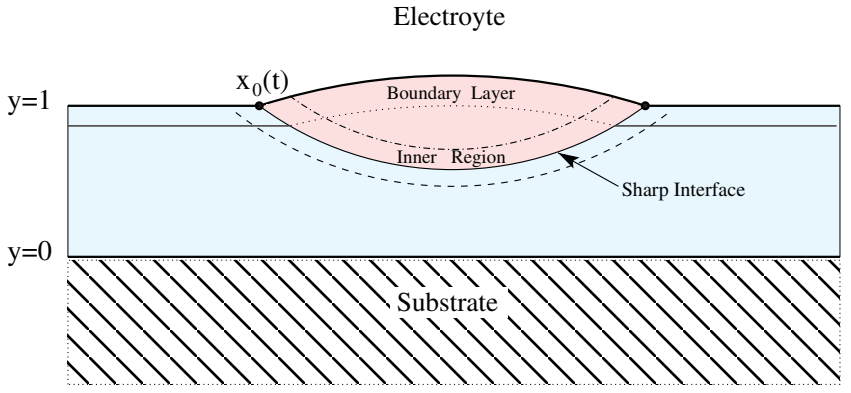

FIGURE 3. Sketch of the layer. We show in pink the lithiated region and we mark the different regions that require a separate treatment: The inner region, the boundary layer and the triple junction point at $x_0(t)$.

For the Cahn–Hilliard equation, we obtain matching powers of ε

$$\nabla^2 \mu_{-1} = 0, \tag{3.2}$$

$$\partial_t c_0 - \nabla^2 \mu_0 = 0. \tag{3.3}$$

No additional equations are necessary. The values of the chemical potential are as follows:

$$\mu_{-1} = f'(c_0), \tag{3.4}$$

$$\mu_0 = f''(c_0) c_1 + \delta\, \partial_c W(u_{i,0}, c_0). \tag{3.5}$$

Note the dependence of μ_0 on the elastic energy. Interpolating functions $h(c)$ and $g(c)$ can be chosen to avoid these terms. This implies

$$h'(c_0^{\pm}) = G'(c_0^{\pm}) = 0, \tag{3.6}$$

where $c_0^{\pm}$ are the values of c_0 on either side of the interface. We will see below that these are constant, and correspond to minima of F. Hence, together with the requirement that the value of F is at a minimum far from the interface, we obtain that c_0 is a constant and $\mu_{-1} = 0$.

The elastic equilibrium equation has the same form to all orders:

$$\nabla \cdot \boldsymbol{\sigma}_m = 0, \tag{3.7}$$

where the index m refers to the order of the expansion. A brief inspection of this equation for $m = -1$ leads to the conclusion that $\boldsymbol{\sigma}_{-1} = 0$, hence we restrict our attention in the outer solution to $m \geqslant 0$.

Finally, the constitutive relation for stress should be written here, the equivalent of equation (2.11*d*), but there is no simple expression valid for every order. Below, we give

Downloaded from https://www.cambridge.org/core. Universitaetsbibliothek, on 26 Oct 2017 at 13:20:02, subject to the Cambridge Core terms of use, available at https://www.cambridge.org/core/terms. https://doi.org/10.1017/S0956792517000067

the formula for the zero-order case for reference. The strain tensor reads

$$\boldsymbol{\epsilon}_0 = \begin{pmatrix} \partial_r u_{r,0} & \frac{1}{2}\left(\partial_s u_{r,0} + \partial_r u_{s,0} - \mathcal{K} u_{s,0}\right) \\ \frac{1}{2}\left(\partial_s u_{r,0} + \partial_r u_{s,0} - \mathcal{K} u_{s,0}\right) & \partial_s u_{s,0} + u_{r,0}\mathcal{K} \end{pmatrix}. \tag{3.8}$$

Similarly, one can derive immediately the form of the stress tensor:

$$\boldsymbol{\sigma}_0 = \frac{2G(c_0)}{1-2\nu}\begin{pmatrix} (1-\nu)\epsilon_{rr,0} + \nu\epsilon_{ss,0} - (1+\nu)h(c_0) & (1-2\nu)\epsilon_{rs,0} \\ (1-2\nu)\epsilon_{rs,0} & (1-\nu)\epsilon_{ss,0} + \nu\epsilon_{rr,0} - (1+\nu)h(c_0) \end{pmatrix}. \tag{3.9}$$

Note that there is a non-zero $\sigma_{zz,0}$ component but it does not intervene in any of the equations due to the plane strain approximation. In the following, we do not consider it.

3.1.2 *Inner expansion*

For the inner variables near the interface, we introduce curvilinear coordinates r and s via the transformations

$$x = X(s,t) + rY'(s,t), \quad y = Y(s,t) - rX'(s,t), \tag{3.10a}$$

with $X'^2 + Y'^2 = 1$, (primes denote differentiation with respect to s and dots with respect to t) and scale r, the coordinate normal to the evolving interface, as $r = \varepsilon\rho$. In terms of these inner coordinates (ρ, s), the operators can be written in the following form:

$$\nabla^2 \to \varepsilon^{-2}\partial_\rho^2 + \varepsilon^{-1}\mathcal{K}\partial_\rho - \rho\mathcal{K}^2\partial_\rho + \partial_s^2 + \cdots, \tag{3.10b}$$

$$\partial_t \to -\frac{v_n}{\varepsilon}\partial_\rho - v_t\partial_s + \partial_t + \cdots, \tag{3.10c}$$

where $\mathcal{K} = X'Y'' - Y'X''$ is the curvature of the interface and $v_n = Y'\dot{X} - X'\dot{Y}$ and $v_t = X'\dot{X} + Y'\dot{Y}$ are the normal and tangential interface velocities. We denote the inner variables with tilde and introduce asymptotic expansions similarly as for the outer problem

$$\tilde{c}(\rho,s,t) = \tilde{c}_0 + \varepsilon\tilde{c}_1 + \varepsilon^2\tilde{c}_2 + \cdots, \tag{3.11a}$$

$$\tilde{\mu}(\rho,s,t) = \varepsilon^{-1}\tilde{\mu}_{-1} + \tilde{\mu}_0 + \varepsilon\tilde{\mu}_1 + \cdots, \tag{3.11b}$$

$$\tilde{u}_i(\rho,s,t) = \tilde{u}_{i,0} + \varepsilon\tilde{u}_{i,1} + \varepsilon^2\tilde{u}_{i,2} + \cdots, \tag{3.11c}$$

$$\tilde{\sigma}_{ij}(\rho,s,t) = \varepsilon^{-1}\tilde{\sigma}_{ij,-1} + \tilde{\sigma}_{ij,0} + \varepsilon\tilde{\sigma}_{ij,1} + \varepsilon^2\tilde{\sigma}_{ij,2} + \cdots \tag{3.11d}$$

We introduce here the *matching conditions*, that allow us to connect the inner and outer expansions. For an arbitrary field ψ, we can expand it in the inner and outer regions as before:

$$\psi(r) = \psi_0(r) + \varepsilon\psi_1(r) + \varepsilon^2\psi_2(r) + \cdots, \tag{3.12a}$$

$$\tilde{\psi}(\rho) = \tilde{\psi}_0(\rho) + \varepsilon\tilde{\psi}_1(\rho) + \varepsilon^2\tilde{\psi}_2(\rho) + \cdots, \tag{3.12b}$$

where only dependence with respect to r is displayed, but the functions can depend on s

Downloaded from https://www.cambridge.org/core. Universitaetsbibliothek, on 26 Oct 2017 at 13:20:02, subject to the Cambridge Core terms of use, available at https://www.cambridge.org/core/terms. https://doi.org/10.1017/S0956792517000067

and t too. The outer expansion can be written as a function of the inner variable ρ and then further expanded in ε:

$$\psi(\varepsilon\rho) = \psi_0^{\pm} + \varepsilon\left(\psi_1^{\pm} + \rho\,\partial_r\psi_0^{\pm}\right) + \varepsilon^2\left(\psi_2^{\pm} + \rho\,\partial_r\psi_1^{\pm} + \frac{1}{2}\rho^2\partial_r^2\psi_0^{\pm}\right) + \cdots, \tag{3.13}$$

where we have introduced the notation

$$\psi^{\pm} = \lim_{r\to\pm 0}\psi(r). \tag{3.14}$$

Notice that ψ can have different functional forms on both (+ and −) sides, we omit that distinction for clarity, and assume that the outer ψ is simply a piecewise-defined function. By a standard argument [28], we equate term by term equations (3.13) and (3.12*b*) in the limit $\rho \to \pm\infty$, obtaining the following matching conditions:

$$\lim_{\rho\to\pm\infty}\left(\tilde{\psi}_0 - \psi_0^{\pm}\right) = 0, \tag{3.15a}$$

$$\lim_{\rho\to\pm\infty}\left(\tilde{\psi}_1 - \psi_1^{\pm} - \rho\,\partial_r\psi_0^{\pm}\right) = 0, \tag{3.15b}$$

$$\lim_{\rho\to\pm\infty}\left(\tilde{\psi}_2 - \psi_2^{\pm} - \rho\,\partial_r\psi_1^{\pm} - \frac{1}{2}\rho^2\partial_r^2\psi_0^{\pm}\right) = 0. \tag{3.15c}$$

Further matching conditions can be extracted from the previous, by means, e.g., of derivation with respect to s.

Note that the previous matching conditions have been derived for a field whose expansion begins with a $O(1)$ term, such as $\tilde{c}$ or $\tilde{u}_i$. In the case of a field which has a $O(\varepsilon^{-1})$ term in its expansion, such as $\tilde{\sigma}_{ij}$ or $\tilde{\mu}$, the same conditions can be derived in a similar way. The end result would be the same as equations (3.15), but after the transformation $\psi_0 \to \psi_{-1}$, etc. Since these conditions are not used, we do not write them explicitly.

We start the inner expansion with the first order of the elastic equilibrium equation, equation (2.11*c*). From the formulas of the appendix, we obtain to order ε^{-2}:

$$(\nabla\cdot\tilde{\boldsymbol{\sigma}})_r = \partial_\rho\tilde{\sigma}_{rr,-1} = 0, \tag{3.16a}$$

$$(\nabla\cdot\tilde{\boldsymbol{\sigma}})_s = \partial_\rho\tilde{\sigma}_{rs,-1} = 0, \tag{3.16b}$$

from which follows that

$$G(\tilde{c}_0)\partial_\rho\tilde{u}_{r,0} = A_r, \tag{3.17a}$$

$$G(\tilde{c}_0)\partial_\rho\tilde{u}_{s,0} = A_s, \tag{3.17b}$$

and hence

$$\tilde{u}_{r,0} = A_r\int_0^\rho \frac{1}{G(\tilde{c}_0)}d\rho' + B_r, \tag{3.18a}$$

$$\tilde{u}_{s,0} = A_s\int_0^\rho \frac{1}{G(\tilde{c}_0)}d\rho' + B_s. \tag{3.18b}$$

Downloaded from https://www.cambridge.org/core. Universitaetsbibliothek, on 26 Oct 2017 at 13:20:02, subject to the Cambridge Core terms of use, available at https://www.cambridge.org/core/terms. https://doi.org/10.1017/S0956792517000067

We will see below that $\tilde{c}_0$ will correspond to a kink-like solution with a bounded range, and $G(\tilde{c}_0)$ is also bounded by construction, as it is constructed as a polynomial function of $\tilde{c}_0$. This implies that both integrals will in general diverge as $\rho \to \infty$, which means, in turn, that it will be impossible to match to the outer solution using equation (3.15*a*) unless $A_r = A_s = 0$. This will also make sure that the displacement field is continuous. The previous result implies that

$$\partial_\rho \tilde{u}_{s,0} = \partial_\rho \tilde{u}_{r,0} = 0, \tag{3.19}$$

and therefore

$$\tilde{\sigma}_{rr,-1} = \tilde{\sigma}_{rs,-1} = \tilde{\sigma}_{sr,-1} = 0.$$

The other component of the stress tensor is also zero to this order ($\tilde{\sigma}_{ss,-1} = 0$). Similarly, the strain tensor to this order is also zero.

In the next order, the elastic equations read as follows:

$$\partial_\rho \tilde{\sigma}_{rr,0} = 0, \quad \partial_\rho \tilde{\sigma}_{rs,0} = 0, \tag{3.20}$$

since the lower order term does not contribute. These equations imply that $\tilde{\sigma}_{rr,0}$ and $\tilde{\sigma}_{rs,0}$ do not depend on ρ. Then, the matching condition (3.15*a*) gives

$$\lim_{\rho \to \pm\infty} \left(\tilde{\sigma}_{ij,0} - \sigma^{\pm}_{ij,0} \right) = 0, \tag{3.21}$$

which implies that $\tilde{\sigma}_{rr,0}$ and $\tilde{\sigma}_{rs,0}$ are continuous. This means that, to zero order, the condition of continuous tractions along the discontinuity is fulfilled. This equation together with the continuity of the displacements ensures a *coherent* interface.

The explicit form of the r, s elements of the strain tensor at this order are as follows:

$$\tilde{\boldsymbol{\epsilon}}_0 = \begin{pmatrix} \partial_\rho \tilde{u}_{r,1} & \frac{1}{2}\left(\partial_s \tilde{u}_{r,0} + \partial_\rho \tilde{u}_{s,1} - \mathcal{K}\tilde{u}_{s,0}\right) \\ \frac{1}{2}\left(\partial_s \tilde{u}_{r,0} + \partial_\rho \tilde{u}_{s,1} - \mathcal{K}\tilde{u}_{s,0}\right) & \partial_s \tilde{u}_{s,0} + \tilde{u}_{r,0}\mathcal{K} \end{pmatrix}. \tag{3.22}$$

Similarly, the stress reads

$$\tilde{\boldsymbol{\sigma}}_0 = \frac{2G(\tilde{c}_0)}{1-2\nu} \begin{pmatrix} (1-\nu)\tilde{\epsilon}_{rr,0} + \nu\tilde{\epsilon}_{ss,0} - (1+\nu)h(\tilde{c}_0) & (1-2\nu)\tilde{\epsilon}_{rs,0} \\ (1-2\nu)\tilde{\epsilon}_{rs,0} & (1-\nu)\tilde{\epsilon}_{ss,0} + \nu\tilde{\epsilon}_{rr,0} - (1+\nu)h(\tilde{c}_0) \end{pmatrix}. \tag{3.23}$$

There is an additional component of stress that is not portrayed, $\tilde{\sigma}_{zz,0}$, but it does not intervene within the plane strain approximation and hence it is ignored.

Equations (3.20), while giving continuity of the tractions $\boldsymbol{\sigma} \cdot \mathbf{n}$ through the interface, they also imply a jump condition on the derivatives of the displacement field. In terms of the displacement field, following equations (3.22) and (3.23), the equations read as follows:

$$\partial_\rho \left[G(\tilde{c}_0) \left((1-\nu)\partial_\rho \tilde{u}_{r,1} + \nu \left(\partial_s \tilde{u}_{s,0} + \tilde{u}_{r,0}\mathcal{K} \right) - (1+\nu)h(\tilde{c}_0) \right) \right] = 0, \tag{3.24a}$$

$$\partial_\rho \left[G(\tilde{c}_0) \left(\partial_s \tilde{u}_{r,0} + \partial_\rho \tilde{u}_{s,1} - \mathcal{K}\tilde{u}_{s,0} \right) \right] = 0. \tag{3.24b}$$

Downloaded from https://www.cambridge.org/core. Universitaetsbibliothek, on 26 Oct 2017 at 13:20:02, subject to the Cambridge Core terms of use, available at https://www.cambridge.org/core/terms. https://doi.org/10.1017/S0956792517000067

These equations can be integrated once and then matched term by term to the outer solution using equations (3.15*a*) and(3.15*b*):

$$G(c_0^{\pm})\left((1-\nu)\partial_r u_{r,0}^{\pm}+\nu\left(\partial_s u_{s,0}+u_{r,0}\mathcal{K}\right)-(1+\nu)h(c_0^{\pm})\right)=K_1(s), \tag{3.25a}$$

$$G(c_0^{\pm})\left(\partial_s u_{r,0}+\partial_r u_{s,0}^{\pm}-\mathcal{K}u_{s,0}\right)=K_2(s). \tag{3.25b}$$

By subtracting the negative limit from the positive limit, we obtain a closed jump condition for the normal derivatives of the displacement field.

For future use, note that (3.19) implies that $\tilde{\epsilon}_{ss,0}$ in equation (3.22) does not depend on ρ, which implies that $\epsilon_{ss,0}^{+}=\epsilon_{ss,0}^{-}$ (i.e. $\epsilon_{ss,0}$ is continuous) by matching condition (3.15*a*).

Once we have found the continuity of $u_{i,0}$ and the continuity of tractions for $\sigma_{ij,0}$, we move on to the Cahn–Hilliard equation. We start by writing down explicitly the form of the chemical potential, by including also the terms coming from equation (A 22) of the appendix:

$$\tilde{\mu}_{-1}=-\partial_\rho^2\tilde{c}_0+f'(\tilde{c}_0), \tag{3.26a}$$

$$\begin{aligned}\tilde{\mu}_0=&-\mathcal{K}\partial_\rho\tilde{c}_0+f''(\tilde{c}_0)\tilde{c}_1-\partial_\rho^2\tilde{c}_1\\&+\frac{\delta}{2}\left[-2h'(\tilde{c}_0)\delta_{ij}\tilde{\sigma}_{ij,0}+\frac{G'(\tilde{c}_0)}{G(\tilde{c}_0)}\left(\tilde{\epsilon}_{ij,0}-h(\tilde{c}_0)\delta_{ij}\right)\tilde{\sigma}_{ij,0}\right],\end{aligned} \tag{3.26b}$$

$$\begin{aligned}\tilde{\mu}_1=&\rho\mathcal{K}^2\partial_\rho\tilde{c}_0-\partial_s^2\tilde{c}_0-\mathcal{K}\partial_\rho\tilde{c}_1+\frac{1}{2}f'''(\tilde{c}_0)\tilde{c}_1^2+f''(\tilde{c}_0)c_2-\partial_\rho^2 c_2\\&+\frac{\delta}{2}\left[-2\left(h'(\tilde{c}_0)\delta_{ij}\sigma_{ij,1}+h''(\tilde{c}_0)\tilde{c}_1\delta_{ij}\tilde{\sigma}_{ij,0}\right)+\frac{G'(\tilde{c}_0)}{G(\tilde{c}_0)}\left(\tilde{\epsilon}_{ij,1}-h'(\tilde{c}_0)\tilde{c}_1\delta_{ij}\right)\tilde{\sigma}_{ij,0}\right.\\&\left.+\frac{G'(\tilde{c}_0)}{G(\tilde{c}_0)}\left(\tilde{\epsilon}_{ij,0}-h(\tilde{c}_0)\delta_{ij}\right)\sigma_{ij,1}+\frac{G''(\tilde{c}_0)G(\tilde{c}_0)-G'(\tilde{c}_0)^2}{G(\tilde{c}_0)^2}\tilde{c}_1\left(\epsilon_{ij,0}-h(\tilde{c}_0)\delta_{ij}\right)\tilde{\sigma}_{ij,0}\right],\end{aligned} \tag{3.26c}$$

note that for $\tilde{\mu}_0$ and $\tilde{\mu}_1$ we only write the non-zero elastic terms. Also, notice that the derivative of the elastic energy does not bring terms of order ε^{-2} to the chemical potential. We now proceed order by order with the Cahn–Hilliard equation:

Order ε^{-3}

To this order, the Cahn–Hilliard equation reads

$$\partial_\rho^2\tilde{\mu}_{-1}=0. \tag{3.27}$$

This means that from equation (3.26*a*), we have

$$\partial_\rho^2\left(-\partial_\rho^2\tilde{c}_0+f'(\tilde{c}_0)\right)=0. \tag{3.28}$$

Following the usual assumptions [28] and making $\tilde{\mu}_{-1}$ a constant, we take a traveling-wave solution of the problem $\tilde{c}_0(\rho)$ such that

$$\lim_{\eta\to\pm\infty}\tilde{c}_0(\rho)=c_0^{\pm}, \tag{3.29}$$

Downloaded from https://www.cambridge.org/core. Universitaetsbibliothek, on 26 Oct 2017 at 13:20:02, subject to the Cambridge Core terms of use, available at https://www.cambridge.org/core/terms. https://doi.org/10.1017/S0956792517000067

i.e. it has two constant limits that match the outer solution, implying that the latter is constant. If we assume that far from the interface the system is in one of the homogeneous equilibria, then $\mu_{-1} = 0$ will be the outer solution with the right boundary conditions. This also implies $\tilde{\mu}_{-1} = 0$.

Order ε^{-2}

To this order, the Cahn–Hilliard equation reads

$$\mathcal{K}\partial_\rho \tilde{\mu}_{-1} - \beta v_n \partial_\rho^3 \tilde{c}_0 + \partial_\rho^2 \tilde{\mu}_0 = 0. \tag{3.30}$$

The first term is zero and the last term can be expanded following equation (3.26*b*):

$$-\beta v_n \partial_\rho^3 \tilde{c}_0 + \partial_\rho^2 \left(-\mathcal{K}\partial_\rho \tilde{c}_0 + f''(\tilde{c}_0)\tilde{c}_1 - \partial_\rho^2 \tilde{c}_1 + \delta\, \partial_{\tilde{c}} \tilde{W}(\tilde{\boldsymbol{\epsilon}}, \tilde{c})_0 \right) = 0, \tag{3.31}$$

with the obvious shorthand

$$\partial_{\tilde{c}} \tilde{W}(\tilde{\boldsymbol{\epsilon}}, \tilde{c})_0 = \frac{1}{2} \left[-2h'(\tilde{c}_0)\delta_{ij}\tilde{\sigma}_{ij,0} + \frac{G'(\tilde{c}_0)}{G(\tilde{c}_0)} \left(\tilde{\epsilon}_{ij,0} - h(\tilde{c}_0)\delta_{ij} \right) \tilde{\sigma}_{ij,0} \right]. \tag{3.32}$$

Equation (3.31) can be integrated twice to yield

$$-\beta v_n \partial_\rho \tilde{c}_0 - \mathcal{K}\partial_\rho \tilde{c}_0 + f''(\tilde{c}_0)\tilde{c}_1 - \partial_\rho^2 \tilde{c}_1 + \delta\, \partial_{\tilde{c}} \tilde{W}(\tilde{\boldsymbol{\epsilon}}, \tilde{c})_0 = A\rho + B, \tag{3.33}$$

with A and B being constants. By matching with the outer solution

$$\lim_{\rho \to \pm\infty} \left(\tilde{c}_1 - c_1^{\pm} - \rho \partial_r c_0^{\pm} \right) = 0, \tag{3.34}$$

and since in curvilinear coordinates, $\partial_r c_0 = 0$, it follows that $\tilde{c}_1$ is bounded if $c_1^{\pm}$ is bounded, and hence $A = 0$ since all the other elements on the left-hand side (LHS) of (3.33) are bounded as $\rho \to \pm\infty$. Alternatively, one can deduce the previous result by matching $\tilde{\mu}_0 - \beta v_n \partial_\rho \tilde{c}_0$ to their outer counterparts. Since $\partial_\rho c_0^{\pm} = \partial_r \mu_{-1}^{\pm} = 0$, we obtain the desired result. To obtain the constant B, equal to $\tilde{\mu}_0 - \beta v_n \partial_\rho \tilde{c}_0$, we notice the following. Equation (3.33) has the form

$$f''(\tilde{c}_0)\tilde{c}_1 - \partial_\rho^2 \tilde{c}_1 = \mathcal{G}. \tag{3.35}$$

It is easy to prove that $\partial_\rho \tilde{c}_0$ is a solution of the homogeneous problem. Since the operator is self-adjoint, and because of the Fredholm alternative, we obtain the following solvability condition:

$$\int_{-\infty}^{\infty} \partial_\rho \tilde{c}_0\, \mathcal{G}\, d\rho = 0. \tag{3.36}$$

This means that

$$(\beta\, v_n + \mathcal{K}) \int_{-\infty}^{+\infty} \left(\partial_\rho \tilde{c}_0 \right)^2 d\rho - \delta \int_{-\infty}^{+\infty} \partial_\rho \tilde{c}_0 \partial_{\tilde{c}} \tilde{W}(\tilde{\boldsymbol{\epsilon}}, \tilde{c})_0\, d\rho + B(c_0^+ - c_0^-) = 0. \tag{3.37}$$

Downloaded from https://www.cambridge.org/core. Universitaetsbibliothek, on 26 Oct 2017 at 13:20:02, subject to the Cambridge Core terms of use, available at https://www.cambridge.org/core/terms. https://doi.org/10.1017/S0956792517000067

Since $\partial_\rho \tilde{c}_0$ goes to zero as $\rho \to \pm\infty$, B matches μ_0. The first integral can be readily performed, but the second one requires a more careful analysis. First, we observe that

$$W^+ - W^- = \int_{-\infty}^{+\infty} \partial_\rho \tilde{c}_0 \, \partial_{\tilde{c}_0} \tilde{W}(\tilde{\boldsymbol{\epsilon}}_0, \tilde{c}_0) \, d\rho + \int_{-\infty}^{+\infty} \partial_\rho \tilde{\epsilon}_{ij,0} \partial_{\tilde{\epsilon}_{ij,0}} \tilde{W}(\tilde{\boldsymbol{\epsilon}}_0, \tilde{c}_0) d\rho, \tag{3.38}$$

which can be obtained from the total derivative of $\tilde{W}$ with respect to ρ (note that $\partial_{\tilde{c}} \tilde{W}(\tilde{\boldsymbol{\epsilon}}, \tilde{c})_0 = \partial_{\tilde{c}_0} \tilde{W}(\tilde{\boldsymbol{\epsilon}}_0, \tilde{c}_0)$). We observe that the first integral is the one that we are interested in, and the second once can be readily computed. First, we notice that

$$\int_{-\infty}^{+\infty} \partial_\rho \tilde{\epsilon}_{ij,0} \, \partial_{\tilde{\epsilon}_{ij,0}} \tilde{W}(\tilde{\boldsymbol{\epsilon}}_0, c_0) \, d\rho = \int_{-\infty}^{+\infty} \partial_\rho \tilde{\epsilon}_{ij,0} \, \tilde{\sigma}_{ij,0} \, d\rho. \tag{3.39}$$

The sum runs over all indices except ss, since this component does not depend on ρ, see above. By integrating by parts, we have that

$$\int_{-\infty}^{+\infty} \partial_\rho \tilde{\epsilon}_{ij,0} \, \tilde{\sigma}_{ij,0} \, d\rho = [\epsilon_{ij,0} \sigma_{ij,0}]_-^+ - \int_{-\infty}^{+\infty} \tilde{\epsilon}_{ij,0} \, \partial_\rho \tilde{\sigma}_{ij,0} \, d\rho, \tag{3.40}$$

but the last integral is zero because of equations (3.20) (note again that the sum excludes $i = s$ and $j = s$). By using the continuity of all $\sigma_{ij,0}$ except $\sigma_{ss,0}$ and because of the continuity of $\epsilon_{ss,0}$, we can write more compactly:

$$\int_{-\infty}^{+\infty} \partial_\rho \tilde{c}_0 \, \partial_{\tilde{c}_0} \tilde{W}(\tilde{\boldsymbol{\epsilon}}_0, \tilde{c}_0) \, d\rho = W^+ - W^- - \sigma_{ij,0}^+ \left(\epsilon_{ij,0}^+ - \epsilon_{ij,0}^- \right), \tag{3.41}$$

where the sum runs over all indices.

Hence, we obtain the following boundary condition:

$$\begin{aligned} \mu_0^\pm (c_0^+ - c_0^-) = &- (\beta \, v_n + \mathcal{K}) \, I + \frac{\delta}{2} \left[\sigma_{ij,0}^+ \left(\epsilon_{ij,0}^+ - \delta_{ij} h(c_0^+) \right) - \sigma_{ij,0}^- \left(\epsilon_{ij,0}^- - \delta_{ij} h(c_0^-) \right) \right] \\ &- \delta \sigma_{ij,0}^+ \left(\epsilon_{ij,0}^+ - \epsilon_{ij,0}^- \right), \end{aligned} \tag{3.42}$$

where I is the integral in (3.37). This same formula without the kinetic term is found in [16]. The last term corresponds to the elastic energy required to maintain coherence at the interface [17,18]. Note that it also implies that μ_0 is continuous, since the right-hand side (RHS) does not change on the side + or the side −.

Order ε^{-1}

To this order, the Cahn–Hilliard equation reads as follows:

$$-v_n \partial_\rho \tilde{c}_0 = \mathcal{K} \partial_\rho \tilde{\mu}_0 - \beta \, v_n \partial_\rho^3 \tilde{c}_1 + \partial_\rho^2 \tilde{\mu}_1 - \beta \, \partial_\rho^2 (v_t \partial_s \tilde{c}_0 - \partial_t \tilde{c}_0) - \beta \, v_n \mathcal{K} \partial_\rho^2 \tilde{c}_0, \tag{3.43}$$

where we have used explicitly $\tilde{\mu}_{-1} = 0$. We can integrate the previous equation once

$$-v_n \tilde{c}_0 = \mathcal{K} \tilde{\mu}_0 - \beta \, v_n \partial_\rho^2 \tilde{c}_1 + \partial_\rho \tilde{\mu}_1 - \beta \, \partial_\rho (v_t \partial_s \tilde{c}_0 - \partial_t \tilde{c}_0) - \beta \, v_n \mathcal{K} \partial_\rho \tilde{c}_0 + C, \tag{3.44}$$

where C is an integration constant, possibly dependent on s. We can take the limit and match the previous equation term by term to the outer solution in the usual way. We

Downloaded from https://www.cambridge.org/core. Universitaetsbibliothek, on 26 Oct 2017 at 13:20:02, subject to the Cambridge Core terms of use, available at https://www.cambridge.org/core/terms. https://doi.org/10.1017/S0956792517000067

obtain, after taking the limit:

$$-v_n c_0^{\pm} = \partial_r \mu_0^{\pm} + \bar{C}, \tag{3.45}$$

where all the terms match to zero or to constants independent of the side of the interface, hence the redefinition of C as $\bar{C}$. From here it is immediate to obtain the conservation condition:

$$\left(c_0^{+} - c_0^{-}\right) v_n = -\left(\partial_r \mu_0^{+} - \partial_r \mu_0^{-}\right). \tag{3.46}$$

3.2 Asymptotic analysis near the absorption boundary

In the following, we assume that the boundary is at $y = 1$ and we define an inner coordinate next to the boundary as

$$\eta = \frac{y-1}{\varepsilon}, \tag{3.47}$$

which implies the transformation $\partial_y \to \varepsilon^{-1}\partial_\eta$. We expand the fields as in the previous case:

$$\hat{c}(x,\eta,t) = \hat{c}_0 + \varepsilon\hat{c}_1 + \varepsilon^2\hat{c}_2 + \cdots, \tag{3.48a}$$

$$\hat{\mu}(x,\eta,t) = \varepsilon^{-1}\hat{\mu}_{-1} + \hat{\mu}_0 + \varepsilon\hat{\mu}_1 + \cdots, \tag{3.48b}$$

$$\hat{u}_i(x,\eta,t) = \hat{u}_{i,0} + \varepsilon\hat{u}_{i,1} + \varepsilon^2\hat{u}_{i,2} + \cdots, \tag{3.48c}$$

$$\hat{\sigma}_{ij}(x,\eta,t) = \varepsilon^{-1}\hat{\sigma}_{ij,-1} + \hat{\sigma}_{ij,0} + \varepsilon\hat{\sigma}_{ij,1} + \varepsilon^2\hat{\sigma}_{ij,2} + \cdots \tag{3.48d}$$

The first two orders for (2.11*a*) in inner coordinates at the boundary are

$$\partial_\eta^2 \hat{\mu}_{-1} = 0, \tag{3.49a}$$

$$\partial_\eta^2 \hat{\mu}_0 = 0. \tag{3.49b}$$

Remarkably, the third condition (2.11*h*) brings in exponentially large terms unless $\hat{\mu}_{-1}$ is zero at the boundary. Hence, we have this boundary condition, together with the matching to the outer solution:

$$\lim_{\eta \to -\infty} \hat{\mu}_{-1} = \mu_{-1} = 0.$$

Together with (3.49*a*), this implies that

$$\hat{\mu}_{-1} = 0. \tag{3.50}$$

The boundary condition for (3.49*b*) then is

$$\partial_\eta \hat{\mu}_0 = 0, \tag{3.51}$$

as once $\hat{\mu}_{-1} = 0$ there are no $O(\varepsilon^{-1})$ terms in the RHS of (2.11*h*). It follows that the solution of equation (3.49*b*) is a constant with respect to η, $\hat{\mu}_0 = \hat{\mu}_0(x)$, thus $\hat{\mu}_0(x)$ is determined by the outer solution via matching, $\mu_0|_{y=1} = \hat{\mu}_0(x)$, rather than vice-versa.

Downloaded from https://www.cambridge.org/core. Universitaetsbibliothek, on 26 Oct 2017 at 13:20:02, subject to the Cambridge Core terms of use, available at https://www.cambridge.org/core/terms. https://doi.org/10.1017/S0956792517000067

The rescaling of (2.11d) to inner coordinates introduces terms of order ε^{-1}, as shown in (3.48d). Introducing this expansion into (2.11c) leads to a problem that at order ε^{-2} reads

$$\partial_\eta \left[G(\hat{c}_0)\partial_\eta \hat{u}_{1,0}\right] = 0, \quad \partial_\eta \left[G(\hat{c}_0)\partial_\eta \hat{u}_{2,0}\right] = 0. \tag{3.52}$$

The boundary conditions (2.11h) for stress give the following relations at order ε^{-1}:

$$G(\hat{c}_0)\partial_\eta \hat{u}_{1,0}|_{y=1} = 0, \quad G(\hat{c}_0)\partial_\eta \hat{u}_{2,0}|_{y=1} = 0. \tag{3.53}$$

Integrating equation (3.52) once and using the previous equation implies that

$$\partial_\eta \hat{u}_{1,0} = 0, \quad \partial_\eta \hat{u}_{2,0} = 0, \tag{3.54}$$

which, in turn, implies that $\hat{\sigma}_{ij,-1} = 0$.

Order ε^{-1}.
To this order, equations (2.11) and (3.50) imply

$$\partial_\eta^2 \hat{\mu}_1 + \beta \partial_\eta^2 \partial_t \hat{c}_0 = 0, \tag{3.55a}$$

$$\partial_\eta^2 \hat{c}_0 - f'(\hat{c}_0) = 0, \tag{3.55b}$$

$$\partial_\eta \hat{\sigma}_{iy,0} = 0, \qquad i = x, y. \tag{3.55c}$$

Regarding the concentration, (3.55b) has to be fulfilled. Notice that no contribution of $\partial_c W$ appears in this equation, as the possible $O(\varepsilon^{-1})$ (and, as matter of fact, $O(\varepsilon^{-2})$) contributions vanish due to (3.54). For (3.55b), we have on the one hand that

$$\lim_{\eta \to -\infty} \hat{c}_0 = c^{\pm},$$

and on the other $\partial_\eta \hat{c}_0|_{\eta=0} = 0$. This implies that

$$\hat{c}_0 = c^{\pm}. \tag{3.56}$$

The previous equation implies that $\partial_t \hat{c}_0 = 0$, and hence equation (3.55a) implies that $\partial_\eta \hat{\mu}_1$ does not depend on η. The boundary condition for $\hat{\mu}_1$ gives

$$\partial_\eta \hat{\mu}_1 = k\left(1 - e^{Q(\mu_0 - \mu_{\text{ext}})}\right). \tag{3.57}$$

Using the matching condition

$$\lim_{\eta \to -\infty} \left(\partial_\eta \hat{\mu}_1 - \partial_y \mu_0|_{y=1}\right) = 0, \tag{3.58}$$

leads to

$$\partial_y \mu_0|_{y=1} = k\left(1 - e^{Q(\mu_0 - \mu_{\text{ext}})}\right), \tag{3.59}$$

that is, $\tilde{\mu}_0$ inherits the boundary condition from the full problem.

Downloaded from https://www.cambridge.org/core. Universitaetsbibliothek, on 26 Oct 2017 at 13:20:02, subject to the Cambridge Core terms of use, available at https://www.cambridge.org/core/terms. https://doi.org/10.1017/S0956792517000067

Integrating (3.55*c*), and using the $O(1)$ approximation of the boundary condition for $\hat{\boldsymbol{\sigma}}$ from (2.11*h*) in inner coordinates, we obtain $\hat{\sigma}_{iy,0} = 0$ for $i = x, y$. Matching then gives the boundary condition

$$\sigma_{iy,0}|_{y=1} = 0, \quad i = x, y, \tag{3.60}$$

for the outer problem for $\boldsymbol{\sigma}_0$.

3.3 Conditions at triple points

We now consider a point where the interface between the two phases meets the boundary of the Silicon domain with the electrolyte following the approach used by [27]. For the boundary located at $y = 1$ so that the layer lies in the region $y < 1$, the triple point is assumed to have the coordinates $x = x_0$ and $y = 1$. We thus rescale according to inner scalings in both Cartesian coordinate directions

$$\xi = \frac{x - x_0(t)}{\varepsilon}, \qquad \eta = \frac{y - 1}{\varepsilon}. \tag{3.61}$$

Rescaling (2.11) gives

$$\varepsilon^2 \partial_t \check{c} - \varepsilon \dot{x}_0 \partial_\xi \check{c} = \nabla^2_{\xi,\eta} \check{\mu} - \beta \dot{x}_0 \nabla^2_{\xi,\eta} \partial_\xi \check{c} + \varepsilon \beta \partial_t \nabla^2_{\xi,\eta} \check{c}, \tag{3.62a}$$

$$\varepsilon \check{\mu} = -\nabla^2_{\xi,\eta} \check{c} + f'(\check{c}) + \varepsilon \partial_{\check{c}} W(\check{\epsilon}_{ij}, \check{c}), \tag{3.62b}$$

where $\nabla^2_{\xi,\eta} = \partial^2_\xi + \partial^2_\eta$. The leading-order problem is

$$\nabla^2_{\xi,\eta} \check{\mu}_0 - \beta \dot{x}_0 \nabla^2_{\xi,\eta} \partial_\xi \check{c}_0 = 0, \tag{3.63a}$$

$$-\nabla^2_{\xi,\eta} \check{c}_0 + f'(\check{c}_0) = 0. \tag{3.63b}$$

The rescaled boundary conditions at $\eta = 0$ are

$$\partial_\eta \check{c} = 0, \qquad \partial_\eta \check{\mu} = \varepsilon k \left(1 - e^{Q(\check{\mu} - \mu_{\text{ext}})}\right), \tag{3.64}$$

thus, to leading order

$$\partial_\eta \check{c}_0 = 0, \qquad \partial_\eta \check{\mu}_0 = 0, \tag{3.65}$$

at $\eta = 0$. Notice that the flux from the non-linear absorption law has dropped out and the problem (3.62), (3.65) is very similar to the one that has been considered for the triple point at a solid wall elsewhere in the literature, e.g., [4]. We summarise the key arguments in the following to recover that the interface between the phases meets the boundary with the electrolyte orthogonally.

Multiply (3.63*b*) with $\partial_\xi \check{c}_0$ and integrate over the box $R \equiv [-R_1/2, R_1/2] \times [-R_2, 0]$, to get

$$\iint_R f'(\check{c}_0)\, \partial_\xi \check{c}_0 \, d\eta d\xi = \iint_R \partial_\xi \check{c}_0 \nabla^2_{\xi,\eta} \check{c}_0 \, d\eta d\xi, \tag{3.66}$$

or

$$\iint_R f'(\check{c}_0) \partial_\xi \check{c}_0 - \partial_\xi \check{c}_0 \partial^2_\xi \check{c}_0 + \partial_\eta \check{c}_0 \partial_{\xi\eta} \check{c}_0 \, d\eta d\xi = \iint_R \partial_\xi \check{c}_0 \partial^2_\eta \check{c}_0 + \partial_\eta \check{c}_0 \partial_{\xi\eta} \check{c}_0 \, d\eta d\xi. \tag{3.67}$$

Downloaded from https://www.cambridge.org/core. Universitaetsbibliothek, on 26 Oct 2017 at 13:20:02, subject to the Cambridge Core terms of use, available at https://www.cambridge.org/core/terms. https://doi.org/10.1017/S0956792517000067

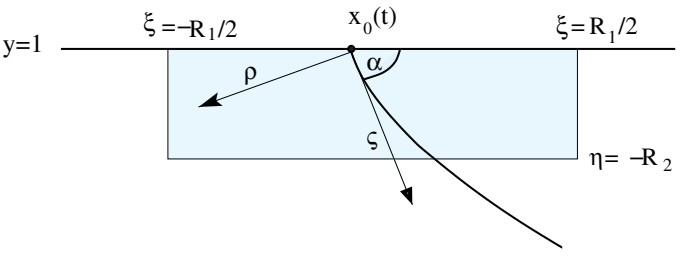

FIGURE 4. Sketch of coordinate system around a triple point.

We now investigate the LHS and RHS of the last equation separately,

$$\text{LHS} = \int_{-R_2}^{0} \left[f(\check{c}_0) - \frac{1}{2}(\partial_\xi \check{c}_0)^2 + \frac{1}{2}(\partial_\eta \check{c}_0)^2 \right]_{\xi=-R_1/2}^{R_1/2} d\eta. \tag{3.68}$$

Taking R_1 and $R_2 \to \infty$ and using that $\partial_\xi \check{c}_0 \to 0$ for $R_1 \to \pm\infty$, we obtain

$$\lim_{R_1,R_2\to\infty} \text{LHS} = \int_{-\infty}^{0} \lim_{R_1\to\infty} \left[f(\check{c}_0) + \frac{1}{2}(\partial_\eta \check{c}_0)^2 \right]_{\xi=-R_1/2}^{R_1/2} d\eta. \tag{3.69}$$

As $\xi \to \pm\infty$, the solution $\check{c}_0$ has to converge to the boundary layer solution at the boundary with the electrolyte, which are the same for both limits except for a change in sign. This, however, does not affect the value of the expression in the square brackets, so in the limit $R_1 \to \infty$ the contributions at $\xi = R_1/2$ and $\xi = -R_1/2$ cancel out, and

$$\lim_{R_1,R_2\to\infty} \text{LHS} = 0. \tag{3.70}$$

For the RHS, we have

$$\text{RHS} = \int_{-R_1/2}^{R_1/2} \left[\partial_\xi \check{c}_0 \, \partial_\eta \check{c}_0 \right]_{\eta=-R_2}^{0} d\xi = \int_{-R_1/2}^{R_1/2} \partial_\xi \check{c}_0 \, \partial_\eta \check{c}_0 \Big|_{\eta=-R_2} d\xi, \tag{3.71}$$

where we have used (3.65) at $\eta = 0$. We now introduce a rotated coordinate system that is aligned with the interface between the phases (see Figure 4), and denote the angle at which this interface meets the boundary with the electrolyte by α. The aim is of course to determine α through the matching. The new coordinates are

$$\rho = -\xi \sin\alpha - \eta \cos\alpha$$
$$\varsigma = \xi \cos\alpha - \eta \sin\alpha,$$

and this gives

$$\text{RHS} = -\int_{\frac{R_1}{2}\sin\alpha + R_2\cos\alpha}^{-\frac{R_1}{2}\sin\alpha + R_2\cos\alpha} S \, d\rho \tag{3.72}$$

with

$$S = \cos\alpha \left((\partial_\rho \check{c}_0)^2 - (\partial_\varsigma \check{c}_0)^2 \right) + \left(\frac{\sin^2\alpha - \cos^2\alpha}{\sin\alpha} \right) \partial_\rho \check{c}_0 \, \partial_\varsigma \check{c}_0. \tag{3.73}$$

Downloaded from https://www.cambridge.org/core. Universitaetsbibliothek, on 26 Oct 2017 at 13:20:02, subject to the Cambridge Core terms of use, available at https://www.cambridge.org/core/terms. https://doi.org/10.1017/S0956792517000067

Since away from the triple point, c varies only slowly along the interface (which is reflected by the fact that for the interface boundary variables, defined in (3.10) only the normal direction is scaled in (3.10*b*), but not s), we need to match $\partial_\varsigma \check{c}_0 \to 0$ as $\varsigma \to \infty$. Thus,

$$\lim_{R_1,R_2\to\infty} \mathrm{RHS} = \lim_{a\to\infty} \lim_{R_1,R_2\to\infty}^{*} \int_{\frac{R_1}{2}\sin\alpha+R_2\cos\alpha}^{-\frac{R_1}{2}\sin\alpha+R_2\cos\alpha} -S\, d\rho, \tag{3.74}$$

where $\lim^*$ is taken under the condition that $|R_1\cos\alpha + R_2\sin\alpha| < a$ (i.e. that the limit for both R_1 and R_2 are carried out simultaneously, i.e. at a similar rate),

$$\lim_{R_1,R_2\to\infty} \mathrm{RHS} = -\cos\alpha \int_{-\infty}^{\infty} \partial_\rho \check{c}_0^2\, d\rho. \tag{3.75}$$

Equating the limits (3.70) and (3.75) and using that the integral in (3.75) is positive, we obtain $\cos\alpha = 0$ i.e., $\alpha = \pi/2$, as expected.

3.4 Sharp-interface model

In summary, the complete sharp-interface model can be written as follows:

$$\nabla^2 \mu_0 = 0, \tag{3.76a}$$

$$\nabla \cdot \boldsymbol{\sigma}_0 = 0, \tag{3.76b}$$

together with the constitutive relation for stress:

$$\sigma_{ij,0} = 2G^{\pm}\left(\epsilon_{ij,0} - \epsilon_{ij}^{0,\pm}\right) + \frac{2\nu}{1-2\nu} G^{\pm}\left(\epsilon_{kk,0} - \epsilon_{kk}^{0,\pm}\right)\delta_{ij}, \tag{3.76c}$$

where $G^{\pm} = G(c_0^{\pm})$ and $\epsilon_{ij}^{0,\pm} = h(c_0^{\pm})$ are constants. The boundary conditions at the free boundary for the elasticity equation correspond to continuity for the elastic field and for the tractions across the interface:

$$\mathbf{u}_0^+ = \mathbf{u}_0^-, \tag{3.76d}$$

$$\mathbf{n}\cdot\boldsymbol{\sigma}_0^+ = \mathbf{n}\cdot\boldsymbol{\sigma}_0^-. \tag{3.76e}$$

For the chemical potential equation, we have at the interface away from the absorption boundary:

$$\mu_0^{\pm}(c_0^+ - c_0^-) = -(\beta v_n + \mathcal{K})I + \frac{\delta}{2}\left[\sigma_{ij,0}^+\left(\epsilon_{ij,0}^+ - \delta_{ij}h(c_0^+)\right) - \sigma_{ij,0}^-\left(\epsilon_{ij,0}^- - \delta_{ij}h(c_0^-)\right)\right] - \delta\,\sigma_{ij,0}^+\left(\epsilon_{ij,0}^+ - \epsilon_{ij,0}^-\right), \tag{3.76f}$$

$$\left(c_0^+ - c_0^-\right) v_n = -\left(\partial_r \mu_0^+ - \partial_r \mu_0^-\right), \tag{3.76g}$$

Downloaded from https://www.cambridge.org/core. Universitaetsbibliothek, on 26 Oct 2017 at 13:20:02, subject to the Cambridge Core terms of use, available at https://www.cambridge.org/core/terms. https://doi.org/10.1017/S0956792517000067

where $I = \int_{-\infty}^{+\infty} \left(\partial_\rho \tilde{c}_0\right)^2 d\rho$. For the conditions at the absorption boundary, we have:

$$\partial_y \mu_0|_{y=1} = k\left(1 - e^{Q(\mu_0 - \mu_{\text{ext}})}\right), \tag{3.76h}$$

$$\sigma_{iy,0}|_{y=1} = 0, \quad i = x, y, \tag{3.76i}$$

and at the triple points the angle is $\alpha = \pi/2$.

Note that in the case of constant flux boundary conditions, we would obtain the same results, except for the exponential factor in equation (3.76*h*), which would not be present.

4 Comparisons to phase-field simulations

We now compare the long-time behaviour of the phase-field model (2.11) with the predictions of the sharp-interface model (3.76). In particular, we are interested in the convergence of the sharp-interface solution to the profile of the chemical potential as a function of the interface thickness ε. For that purpose, we have computed numerically the solution of the phase-field model in the one-dimensional case. We have used the constant flux boundary condition and linear interpolating functions $h(c) = g(c) = c$ for simplicity. This choice does not change the equations for μ_0 in the sharp interface limit. The simulations are performed using a non-linear adaptive multigrid algorithm [32]. For details on the simulations, see [23].

Figure 5 summarizes the effect of parameters β and δ on the convergence. The solutions of the sharp interface model to leading order in μ are straight lines in one dimension, meeting at the interface. Dashed lines in this figure fit μ far enough from the inner region, at a distance of 15ε from the point where $c_0 = 1/2$, and over an interval of width 0.05. These lines provide an approximation to the sharp interface limit solution. On top, we see that the value of ε and the value of δ have a strong effect on the quality of the fit. On the one hand, for the moderate value of δ, we obtain the expected result, i.e. the inner region becomes narrower with smaller values of ε and the convergence improves, this improvement of the convergence is also reflected in the value of μ at $y = 1$. On the other hand, for $\delta = 10.0$ we see how, while there appears to be some convergence, the solution curves are far from being straight lines. This of course indicates that the sharp interface model is far from valid for such high values of the parameter δ, and a much smaller ε is needed to observe convergence.

On the bottom of Figure 5, we see the effect of β. For the higher value of β, we have a good convergence, and the inner region becomes narrower as ε decreases. Nevertheless, the effect of β is clear, in that there is a depression near the point where both dashed lines meet. This is well represented by the expansion in the inner region. Indeed, in the inner expansion, the Cahn–Hilliard equation contains at order ε^{-2} a source term proportional to β (see equation 3.30), and hence this result is to be expected. For $\beta = 0.05$, the smallest value, we see how this depression in the inner region has disappeared and the agreement with the linear fits is extremely good.

In Figure 6, we quantify how good is the agreement between the sharp interface and the phase-field model by using a sharp interface relation, equation (3.76*g*), and computing how well it is approximated by the quantities extracted from the phase-field model. We compute numerically the gradients of the chemical potential from the fitting lines in

Downloaded from https://www.cambridge.org/core. Universitaetsbibliothek, on 26 Oct 2017 at 13:20:02, subject to the Cambridge Core terms of use, available at https://www.cambridge.org/core/terms. https://doi.org/10.1017/S0956792517000067

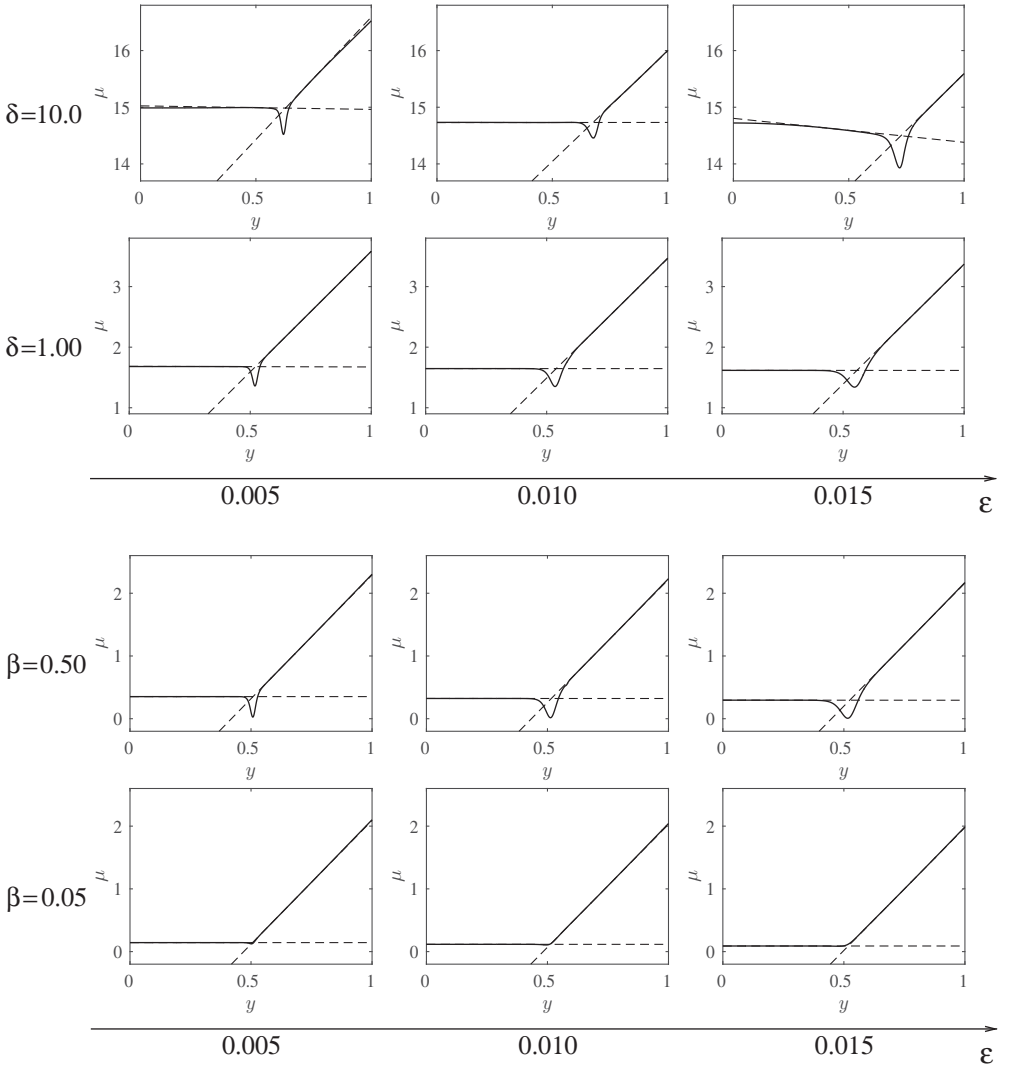

FIGURE 5. Convergence to the sharp interface limit. Solid lines correspond to the chemical potential μ on the layer, dashed lines correspond to a linear fit near the interface to compute the derivatives. Top: Results for two values of δ, $\beta = 0.5$. Bottom: Results for two values of the kinetic parameter β, $\delta = 0.1$. All results were obtained with fixed flux boundary conditions for μ.

Figure 5 and the velocity of the advancing front. The ratio of the jump in the derivative and the velocity in the sharp-interface model is equal to one. We compute this ratio numerically in the phase-field model and represent the results for $\beta = 0.05$ and $\beta = 0.5$ as a function of ε, and the convergence found is very good. The parabola that fits the $\beta = 0.05$ case also gives a very good approximation to the $\beta = 0.5$ case, except for the highest value of ε, and has a crossing point with the vertical axis at $\varepsilon = 0$ with a value of 1.00028.

Downloaded from https://www.cambridge.org/core. Universitaetsbibliothek, on 26 Oct 2017 at 13:20:02, subject to the Cambridge Core terms of use, available at https://www.cambridge.org/core/terms. https://doi.org/10.1017/S0956792517000067

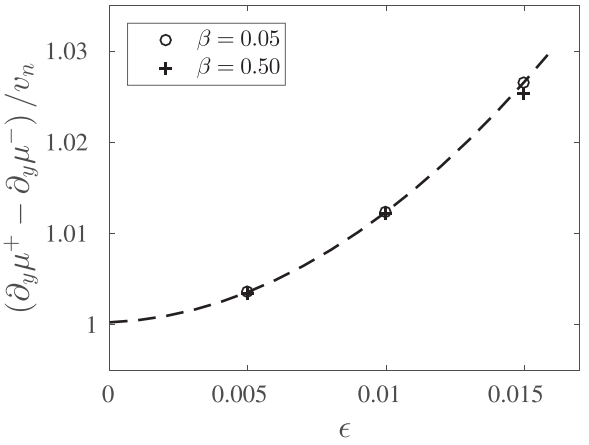

FIGURE 6. Convergence to the sharp interface limit, for two values of the kinetic parameter β. Symbols correspond to the ratio of the expected velocity to the measured front velocity. The dashed line is a parabolic fit to the $\beta = 0.05$ symbols. With fixed flux boundary conditions, $\delta = 0.1$. (non-dimensional units)

This very good agreement and the quadratic convergence seem to indicate, in accordance with similar results in other systems, e.g., Ref. [24], that the smallest order of the finite ε corrections to equation (3.76g) will be $O(\varepsilon^2)$.

5 Conclusion

Understanding the conditions that cause the deformation and eventual destruction of silicon electrode particles during intercalation is a prerequisite to optimizing design and loading conditions. In this regard, it is interesting to be able to follow the structure formation and thus the non-uniform stress evolution of a silicon electrode particle in detail and on long-time scales as a function of the control parameters, such as the ion flux rate or the ratio of elastic to interfacial energies. In particular, the sharp-interface model that we have derived in this study allows for more analytical insight into the complex intercalation process. Except for extremely low lithiation rates, the time scale on which the sharp-interface dynamics takes place is the relevant time scale for comparison with experimental results on the lithiation process.

Results of the comparison of the long-time dynamics of the phase-field model and the velocity deduced from the sharp interface model show a good quadratic convergence in epsilon, in particular for smaller values of the ratio of elastic to interfacial energies. These are encouraging results, and provide a means to validate the range of parameters in which the phase-field model gives physically robust results.

Additionally, we have incorporated the study of non-linear boundary conditions at the adsorption boundary to the study of the sharp-interface limit. The boundary conditions considered capture the complexity of the real boundary conditions for the problem at hand, and in this work we have proven that their form remains essentially invariant in the sharp-interface limit.

Downloaded from https://www.cambridge.org/core. Universitaetsbibliothek, on 26 Oct 2017 at 13:20:02, subject to the Cambridge Core terms of use, available at https://www.cambridge.org/core/terms. https://doi.org/10.1017/S0956792517000067

Natural extensions of this work will include the stability of the moving lithiation front and the coarsening mechanisms of the evolving structures. For a more realistic model effects of charge and electrical potential will have to be included, but at this stage our aim was first to understand the role of non-homogeneous elasticity in the stress-lithiation curve, see [23]. In addition, the underlying phase-field model is only applicable for regimes that depart little from equilibrium, and we are actually considering non-equilibrium phase transitions between what can be at best characterized as metastable states.

With the current model, comparisons to experiments can only be qualitative since we have made the simplifying assumption of linear elasticity. However, we will include finite strain effects in our upcoming research.

Acknowledgements

This research was carried out in the framework of MATHEON supported by the Einstein Foundation Berlin.

References

[1] ABELS, H. & SCHAUBECK, S. (2015) Sharp interface limit for the Cahn-Larché system. *Asymptotic Anal.* **91**(3–4), 283–340.

[2] BAZANT, M. Z. (2013) Theory of chemical kinetics and charge transfer based on nonequilibrium thermodynamics. *Acc. Chem. Res.* **46**(5), 1144–1160.

[3] BOWER, A. F., GUDURU, P. R. & SETHURAMAN, V. A. (2011) A finite strain model of stress, diffusion, plastic flow, and electrochemical reactions in a lithium-ion half-cell. *J. Mech. Phys. Solids* **59**(4), 804–828.

[4] BRONSARD, L., GARCKE, H. & STOTH, B. (1998) A multi-phase Mullins-Sekerka system: Matched asymptotic expansions and an implicit time discretisation or the geometric evolution problem. *Proc. Roy. Soc. of Edingburgh: Sec. A Math.* **128**, 481–06.

[5] BUCCI, G., NADIMPALLI, S. P., SETHURAMAN, V. A., BOWER, A. F. & GUDURU, P. R. (2014) Measurement and modeling of the mechanical and electrochemical response of amorphous Si thin film electrodes during cyclic lithiation. *J. Mech. Phys. Solids* **62**, 276–294.

[6] BURCH, D. & BAZANT, M. Z. (2009) Size-dependent spinodal and miscibility gaps for intercalation in nanoparticles. *Nano Lett.* **9**(11), 3795–3800, pMID: 19824617.

[7] CHAKRABORTY, J., PLEASE, C. P., GORIELY, A. & CHAPMAN, S. J. (2015) Combining mechanical and chemical effects in the deformation and failure of a cylindrical electrode particle in a Li-ion battery. *International Journal of Solids and Structures* **54**, 66–81.

[8] CHAKRABORTY, J., PLEASE, C. P., GORIELY, A. & CHAPMAN, S. J. (2015) Influence of constraints on axial growth reduction of cylindrical Li-ion battery electrode particles. *J. Power Sources* **279**, 746–758, 9th International Conference on Lead-Acid Batteries (LABAT) 2014.

[9] CUBUK, E. D. & KAXIRAS, E. (2014) Theory of structural transformation in lithiated amorphous silicon. *Nano Lett.* **14**(7), 4065–4070.

[10] CUI, Z., GAO, F. & QU, J. (2012) A finite deformation stress-dependent chemical potential and its applications to lithium ion batteries. *Journal of the Mechanics and Physics of Solids* **60**(7), 1280–1295.

[11] FRATZL, P., PENROSE, O. & LEBOWITZ, J. L. (1999) Modeling of phase separation in alloys with coherent elastic misfit. *J. Stat. Phys.* **95**(5-6), 1429–1503.

[12] FRIED, E. & GURTIN, M. E. (1994) Dynamic solid-solid transitions with phase characterized by an order parameter. *Physica D: Nonlinear Phenom.* **72**(4), 287–308.

[13] GARCKE, H. (2003) On Cahn-Hilliard systems with elasticity. *Proc. Edinburgh: Sect. A Math.* **133**(02), 307–331.

Downloaded from https://www.cambridge.org/core. Universitaetsbibliothek, on 26 Oct 2017 at 13:20:02, subject to the Cambridge Core terms of use, available at https://www.cambridge.org/core/terms. https://doi.org/10.1017/S0956792517000067

[14] Garcke, H. & Kwak, D. J. C. (2006) On asymptotic limits of Cahn-Hilliard systems with elastic misfit. In: A. Mielke (editor), *Analysis, Modeling and Simulation of Multiscale Problems*, Springer, Berlin, pp. 87–111.

[15] Huang, Y., Ngo, D. & Rosakis, A. (2005) Non-uniform, axisymmetric misfit strain: In thin films bonded on plate substrates/substrate systems: The relation between non-uniform film stresses and system curvatures. *Acta Mech. Sin.* **21**(4), 362–370.

[16] Leo, P., Lowengrub, J. & Jou, H.-J. (1998) A diffuse interface model for microstructural evolution in elastically stressed solids. *Acta Mater.* **46**(6), 2113–2130.

[17] Leo, P. & Sekerka, R. (1989) Overview no. 86: The effect of surface stress on crystal-melt and crystal-crystal equilibrium. *Acta Metall.* **37**(12), 3119–3138.

[18] Leo, P. H. & Sekerka, R. (1989) The effect of elastic fields on the morphological stability of a precipitate grown from solid solution. *Acta Metall.* **37**(12), 3139–3149.

[19] Levitas, V. I. & Attariani, H. (2014) Anisotropic compositional expansion in elastoplastic materials and corresponding chemical potential: Large-strain formulation and application to amorphous lithiated silicon. *J. Mech. Phys. Solids* **69**, 84–111.

[20] Liu, X. H., Fan, F., Yang, H., Zhang, S., Huang, J. Y. & Zhu, T. (2013) Self-limiting lithiation in silicon nanowires. *ACS Nano* **7**(2), 1495–1503.

[21] McDowell, M. T., Lee, S. W., Harris, J. T., Korgel, B. A., Wang, C., Nix, W. D. & Cui, Y. (2013) In situ tem of two-phase lithiation of amorphous silicon nanospheres. *Nano Lett.* **13**(2), 758–764.

[22] McDowell, M. T., Lee, S. W., Nix, W. D. & Cui, Y. (2013) 25th anniversary article: Understanding the lithiation of silicon and other alloying anodes for lithium-ion batteries. *Adv. Mater.* **25**(36), 4966–4985.

[23] Meca, E., Münch, A. & Wagner, B. (2016) Thin-film electrodes for high-capacity lithium-ion batteries: Influence of phase transformations on stress. *Proc. R. Soc. A: Math. Phys. Eng. Sci.* **472**(2193), 20160093.

[24] Meca, E., Shenoy, V. B. & Lowengrub, J. (2013) Phase-field modeling of two-dimensional crystal growth with anisotropic diffusion. *Phys. Rev. E* **88**, 052409.

[25] Ngo, D., Huang, Y., Rosakis, A. & Feng, X. (2006) Spatially non-uniform, isotropic misfit strain in thin films bonded on plate substrates: The relation between non-uniform film stresses and system curvatures. *Thin Solid Films* **515**(4), 2220–2229.

[26] Novick-Cohen, A. (1988) On the viscous Cahn-Hilliard equation. Material instabilities in continuum mechanics, Edinburgh, 1985–1986, Oxford Sci. Publ., Oxford Univ. Press, New York, pp. 329–342.

[27] Owen, N., Rubinstein, J. & Sternberg, P. (1990) Minimizers and gradient flows for singularly perturbed bi-stable potentials with a Dirichlet condition. *Proc. R. Soc. Lond. A* **429**, 505–532.

[28] Pego, R. L. (1989) Front migration in the nonlinear Cahn-Hilliard equation. *Proc. R. Soc. London A: Math. Phys. Eng. Sci.* **422**(1863), 261–278.

[29] Sethuraman, V. A., Chon, M. J., Shimshak, M., Srinivasan, V. & Guduru, P. R. (2010) In situ measurements of stress evolution in silicon thin films during electrochemical lithiation and delithiation. *J. Power Sources* **195**(15), 5062–5066.

[30] Shenoy, V., Johari, P. & Qi, Y. (2010) Elastic softening of amorphous and crystalline Li–Si phases with increasing Li concentration: A first-principles study. *J. Power Sources* **195**(19), 6825–6830.

[31] Wang, J. W. *et al.* (2013) Two-phase electrochemical lithiation in amorphous silicon. *Nano Lett.* **13**(2), 709–715.

[32] Wise, S., Kim, J. & Lowengrub, J. (2007) Solving the regularized, strongly anisotropic Cahn-Hilliard equation by an adaptive nonlinear multigrid method. *J. Comput. Phys.* **226**(1), 414 – 446.

[33] Zeng, Y. & Bazant, M. Z. (2014) Phase separation dynamics in isotropic ion-intercalation particles. *SIAM J. Appl. Math.* **74**(4), 980–1004.

Downloaded from https://www.cambridge.org/core. Universitaetsbibliothek, on 26 Oct 2017 at 13:20:02, subject to the Cambridge Core terms of use, available at https://www.cambridge.org/core/terms. https://doi.org/10.1017/S0956792517000067

[34] Zhao, K., Tritsaris, G. A., Pharr, M., Wang, W. L., Okeke, O., Suo, Z., Vlassak, J. J. & Kaxiras, E. (2012) Reactive flow in silicon electrodes assisted by the insertion of lithium. *Nano Lett.* **12**(8), 4397–4403.

Appendix A Curvilinear coordinates

In this appendix, the change of coordinates used in Section 3.1 is explained in detail, including the resulting form of the differential operators. The interface is defined by the functions X and Y, which depend on the arclength s and time t. Based on these two functions, a coordinate system can be defined in terms of the arclength and the distance to the interface r:

$$x = X(s,t) + rY'(s,t), \tag{A 1}$$

$$y = Y(s,t) - rX'(s,t), \tag{A 2}$$

where the prime denotes differentiation with respect to s and $X'(s,t)^2 + Y'(s,t)^2 = 1$. We omit the t argument from now on for clarity. It is easy to prove that the curvature of the interface is $\mathcal{K} = X'(s)Y''(s) - Y'(s)X''(s)$. The interface is considered to be independent of z, in accordance with the plane strain approximation that is used through this work.

Differentiating with respect to r and s defines the natural basis:

$$\mathbf{g}_1 = \begin{pmatrix} Y'(s) \\ -X'(s) \end{pmatrix}, \quad \mathbf{g}_2 = \begin{pmatrix} X'(s) + rY''(s) \\ Y'(s) - rX''(s) \end{pmatrix}. \tag{A 3}$$

And the physical basis is defined in terms of unitary vectors:

$$\hat{\mathbf{r}} \equiv \mathbf{e}_r = \mathbf{g}_1, \quad \hat{\mathbf{s}} \equiv \mathbf{e}_s = \frac{\mathbf{g}_2}{\|\mathbf{g}_2\|} = \frac{1}{\mathfrak{h}}\mathbf{g}_2, \tag{A 4}$$

where $\mathfrak{h} = 1 + r\mathcal{K}$.

The dual basis can easily be computed:

$$\mathbf{g}^1 = \mathbf{g}_1, \quad \mathbf{g}^2 = \frac{\mathbf{g}_2}{\mathfrak{h}^2}. \tag{A 5}$$

Note that all the previous definitions ignore the z component, for which $\mathbf{g}_3 = \mathbf{g}^3 = \mathbf{e}_z$. We do not incorporate the z component in vectors and tensors since it is usually trivial.

A.1 Gradient of a scalar

$$\nabla f = \partial_k f \mathbf{g}^k = \partial_r f \hat{\mathbf{r}} + \frac{1}{\mathfrak{h}}\partial_s f \hat{\mathbf{s}}. \tag{A 6}$$

A.2 Gradient of a vector

$$\nabla \mathbf{v} = \left(\partial_k v^i + v^j \Gamma^i_{jk}\right) \mathbf{g}_i \otimes \mathbf{g}^k. \tag{A 7}$$

Downloaded from https://www.cambridge.org/core. Universitaetsbibliothek, on 26 Oct 2017 at 13:20:02, subject to the Cambridge Core terms of use, available at https://www.cambridge.org/core/terms. https://doi.org/10.1017/S0956792517000067

The Christoffel symbols of the second kind Γ^i_{jk} can be defined by the formula

$$\Gamma^i_{jk} = \mathbf{g}^i \cdot \partial_k \mathbf{g}_j.$$

It can be proved that all of the Γ^i_{jk} are zero except for

$$\Gamma^2_{12} = \Gamma^2_{21} = \frac{\mathcal{K}}{\mathfrak{h}},$$
$$\Gamma^1_{22} = -\mathcal{K}\mathfrak{h},$$
$$\Gamma^2_{22} = \frac{r\mathcal{K}'}{\mathfrak{h}}.$$

In order to derive the previous formulas, an extensive use has been made of the formula $X'(s)^2 + Y'(s)^2 = 1$ and its derivatives with respect to s. We give as an example the derivation of the value of Γ^1_{22}:

$$\Gamma^1_{22} = \mathbf{g}^1 \cdot \partial_s \mathbf{g}_2 = Y'X'' - X'Y'' + r(Y'Y''' + X'X'''). \tag{A 8}$$

By using the expansion of $(X'^2 + Y'^2)'' = 0$, we obtain

$$\Gamma^1_{22} = -\mathcal{K} - r(X''^2 + Y''^2) = -\mathcal{K}(1 + r\mathcal{K}) = -\mathcal{K}\mathfrak{h}, \tag{A 9}$$

where we have used $\mathcal{K}^2 = (X''^2 + Y''^2)$, which can be easily proved using the definition of $\mathcal{K}$ and the expansion of $(X'^2 + Y'^2)' = 0$.

The components of $\nabla \mathbf{v}$ in the natural basis read thus as follows:

$$(\nabla \mathbf{v})^i_k = \begin{pmatrix} \partial_r v^1 & \partial_s v^1 - v^2 \mathcal{K}\mathfrak{h} \\ \partial_r v^2 + v^2 \dfrac{\mathcal{K}}{\mathfrak{h}} & \partial_s v^2 + v^1 \dfrac{\mathcal{K}}{\mathfrak{h}} + v^2 \dfrac{r\mathcal{K}'}{\mathfrak{h}} \end{pmatrix}. \tag{A 10}$$

In the physical basis, these elements can be readily computed:

$$\begin{pmatrix} \partial_r v^r & \dfrac{1}{\mathfrak{h}}(\partial_s v^r - v^s \mathcal{K}) \\ \mathfrak{h}\partial_r\left(\dfrac{v^s}{\mathfrak{h}}\right) + v^s \dfrac{\mathcal{K}}{\mathfrak{h}} & \dfrac{1}{\mathfrak{h}}(\partial_s v^s + v^r \mathcal{K}) \end{pmatrix}. \tag{A 11}$$

Note that the physical components are related to the natural components as follows: $v^1 \mathbf{g}_1 = v^r \hat{\mathbf{r}}$ and $v^2 \mathbf{g}_2 = v^s \hat{\mathbf{s}}$ imply that $v^r = v^1$ and $v^s = \mathfrak{h} v^2$. The same is true for rank-2 tensors, e.g., $\mathrm{S}^2_1 \mathbf{g}_2 \otimes \mathbf{g}^1 = \mathrm{S}^s_r \hat{\mathbf{s}} \otimes \hat{\mathbf{r}}$ implies that $\mathrm{S}^2_1 = \mathrm{S}^s_r / \mathfrak{h}$.

A.3 Divergence of a second-order tensor field

$$\nabla \cdot \mathrm{S} = \left(\partial_i \mathrm{S}^i_j + \mathrm{S}^l_j \Gamma^i_{il} - \mathrm{S}^i_l \Gamma^l_{ij}\right) \mathbf{g}^j. \tag{A 12}$$

Downloaded from https://www.cambridge.org/core. Universitaetsbibliothek, on 26 Oct 2017 at 13:20:02, subject to the Cambridge Core terms of use, available at https://www.cambridge.org/core/terms. https://doi.org/10.1017/S0956792517000067

By expanding the previous formula and introducing the values of the Christoffel symbols the following expression is derived:

$$(\nabla \cdot \mathrm{S})_1 = \partial_1 \mathrm{S}_1^1 + \partial_2 \mathrm{S}_1^2 + \mathrm{S}_1^1 \frac{\mathcal{K}}{\mathfrak{h}} + \mathrm{S}_1^2 \frac{r\mathcal{K}'}{\mathfrak{h}} - \mathrm{S}_2^2 \frac{\mathcal{K}}{\mathfrak{h}}, \tag{A 13}$$

$$(\nabla \cdot \mathrm{S})_2 = \partial_1 \mathrm{S}_2^1 + \partial_2 \mathrm{S}_2^2 + \mathfrak{h}\mathrm{S}_1^2 \mathcal{K}. \tag{A 14}$$

In terms of the physical components, we have

$$(\nabla \cdot \mathrm{S})_r = \partial_r \mathrm{S}_r^r + \frac{1}{\mathfrak{h}} \partial_s \mathrm{S}_r^s + \mathrm{S}_r^r \frac{\mathcal{K}}{\mathfrak{h}} - \mathrm{S}_s^s \frac{\mathcal{K}}{\mathfrak{h}}, \tag{A 15}$$

$$(\nabla \cdot \mathrm{S})_s = \mathfrak{h}\partial_r \left(\mathfrak{h}\mathrm{S}_s^r\right) + \mathfrak{h}\partial_s \mathrm{S}_s^s + \mathfrak{h}\mathrm{S}_r^s \mathcal{K}. \tag{A 16}$$

A.4 Tensors from the theory of elasticity

From equation (A 11), we can compute the strain tensor in these coordinates:

$$\boldsymbol{\epsilon} = \frac{1}{2}\left(\nabla \mathbf{u} + \nabla \mathbf{u}^T\right) = \begin{pmatrix} \partial_r u^r & \frac{1}{2}\left(\frac{1}{\mathfrak{h}}\partial_s u^r + \mathfrak{h}\partial_r\left(\frac{u^s}{\mathfrak{h}}\right)\right) \\ \frac{1}{2}\left(\frac{1}{\mathfrak{h}}\partial_s u^r + \mathfrak{h}\partial_r\left(\frac{u^s}{\mathfrak{h}}\right)\right) & \frac{1}{\mathfrak{h}}\left(\partial_s u^s + u^r \mathcal{K}\right) \end{pmatrix}. \tag{A 17}$$

Since the new coordinates are orthogonal and are related with the old ones through a rotation (locally) and the elasticity tensor C_{ijkl} is invariant with respect to rotations, equation (2.11*d*) is still valid. We can write the elements of the stress tensor explicitly:

$$\begin{aligned} \sigma_{rr} &= \frac{2G}{1-2v}\left((1-v)\epsilon_{rr} + v\epsilon_{ss} - (1+v)h(c)\right) \\ &= \frac{2G}{1-2v}\left((1-v)\partial_r u^r + \frac{v}{\mathfrak{h}}\left(\partial_s u^s + u^r \mathcal{K}\right) - (1+v)h(c)\right), \end{aligned} \tag{A 18}$$

$$\sigma_{rs} = \sigma_{sr} = 2G\epsilon_{rs} = G\left(\frac{1}{\mathfrak{h}}\partial_s u^r + \mathfrak{h}\partial_r\left(\frac{u^s}{\mathfrak{h}}\right)\right), \tag{A 19}$$

$$\begin{aligned} \sigma_{ss} &= \frac{2G}{1-2v}\left((1-v)\epsilon_{ss} + v\epsilon_{rr} - (1+v)h(c)\right) \\ &= \frac{2G}{1-2v}\left(v\partial_r u^r + \frac{1-v}{\mathfrak{h}}\left(\partial_s u^s + u^r \mathcal{K}\right) - (1+v)h(c)\right). \end{aligned} \tag{A 20}$$

In order to write the equations, it is important to obtain the value of the derivative of the elastic energy (equation (2.1)). It can be written as follows:

$$\partial_c W(\boldsymbol{\epsilon}, c) = \frac{1}{2}\left[-2h'(c)\delta_{ij}\sigma_{ij} + \frac{G'(c)}{G(c)}\left(\epsilon_{ij} - h(c)\delta_{ij}\right)\sigma_{ij}\right], \tag{A 21}$$

where the indices run over r, s and z. When written in terms of the displacement field, the

Downloaded from https://www.cambridge.org/core. Universitaetsbibliothek, on 26 Oct 2017 at 13:20:02, subject to the Cambridge Core terms of use, available at https://www.cambridge.org/core/terms. https://doi.org/10.1017/S0956792517000067

derivative reads as follows:

$$\begin{aligned}\partial_c W(\boldsymbol{\epsilon}, c) = {} & (1+\nu)\frac{3(h(c)^2 G(c))'}{1-2\nu} \\ & + \frac{(1-\nu)G'(c)}{1-2\nu}\left[(\partial_r u^r)^2 + \frac{1}{\mathfrak{h}^2}\left(\partial_s u^s + u^r \mathcal{K}\right)^2\right] \\ & + \frac{1}{\mathfrak{h}}\frac{2\nu G'(c)}{1-2\nu}\partial_r u^r \left(\partial_s u^s + u^r \mathcal{K}\right) \\ & - \frac{2(1+\nu)(h(c)G(c))'}{1-2\nu}\left[\partial_r u^r + \frac{1}{\mathfrak{h}}\left(\partial_s u^s + u^r \mathcal{K}\right)\right] \\ & + \frac{1}{2}G'(c)\left(\frac{1}{\mathfrak{h}}\partial_s u^r + \mathfrak{h}\partial_r\left(\frac{u^s}{\mathfrak{h}}\right)\right)^2.\end{aligned} \tag{A 22}$$

Downloaded from https://www.cambridge.org/core. Universitaetsbibliothek, on 26 Oct 2017 at 13:20:02, subject to the Cambridge Core terms of use, available at https://www.cambridge.org/core/terms. https://doi.org/10.1017/S0956792517000067